

AD-A214 573

FLEXIBILITY OF THE ZEOLITE RHO FRAMEWORK.
IN SITU X-RAY AND NEUTRON POWDER STRUCTURAL
CHARACTERIZATION OF DIVALENT CATION-EXCHANGED
ZEOLITE RHO

D. R. Corbin, L. Abrams, and G. A. Jones

Central Research and Development Department*
E. I. du Pont de Nemours and Company, Inc.
Experimental Station
P. O. Box 80262
Wilmington, DE 19880-0262

M. M. Eddy, W. T. A. Harrison, and G. D. Stucky

Department of Chemistry
University of California at Santa Barbara
Santa Barbara, CA 93106

D. E. Cox

Physics Department
Brookhaven National Laboratory
Long Island, Upton, NY 11973

DTIC
ELECTE
NOV 16 1989
S E D

This document has been approved
for public release and sale.
Distribution is unlimited.

* Contribution Number 4930

89 11 15 039

ABSTRACT

Zeolite RHO has an unusual three dimensional monolayer surface with a topology that gives equal access to either side of the surface. In the absence of supporting structural subunits, e.g., smaller cages or channels, RHO exhibits atypical framework flexibility with large displacive rearrangements. These have been investigated by in situ X-ray powder diffraction studies of zeolite RHO exchanged with various divalent cations. The unit cell variation (e.g., Ca,H-RHO(400°C), $a = 13.970(5)\text{\AA}$; Sr-RHO(250°C), $a = 14.045(1)\text{\AA}$; Ba-RHO(200°C), $a = 14.184(2)\text{\AA}$; Cd-RHO(350°C), $a = 14.488(3)\text{\AA}$; Na,Cs-RHO(25°C), $a = 15.031\text{\AA}$) is a particularly sensitive function of cation and temperature. Rietveld analysis of neutron diffraction data was used to refine the structures of two samples, Ca,ND₄-RHO and Ca,D-RHO. Ca,D-RHO shows the largest reported deviation from Im3m symmetry ($a = 13.9645(7)\text{\AA}$) for a RHO structure. The calcium atom is located in the center of the double 8-ring, distorting the framework to generate a tetrahedral environment. The results confirm one of the largest displacive distortions observed for a molecular sieve framework with a unit cell volume increase of 25% when the calcium ions of Ca,H-RHO are replaced with hydrogen ions to give H-RHO.

Accession For	
NTIS GRA&I	<input checked="" type="checkbox"/>
DTIC TAB	<input type="checkbox"/>
Unannounced	<input type="checkbox"/>
Justification	
By	
Distribution/	
Availability Codes	
Dist	Avail and/or Special
A-1	



INTRODUCTION

Zeolites are crystalline aluminosilicate materials with open framework structures of molecular dimensions. The term "open framework" indicates the presence of intracrystalline voids - that is, cages and channels or pore openings. It is the shape and size of these pore openings that give a zeolite its molecular sieving ability and hence shape and size selectivity when used as a catalyst, support, or absorbent. It is generally accepted that the framework and hence the pore openings of the zeolite are rigid. However, several zeolite frameworks have been shown to exhibit small distortions with change of symmetry on sorption of different solvents¹ or as a function of temperature.² The observed distortions and their effects on the pore openings are insignificant when compared to the flexibility and distortions observed in the framework of zeolite RHO.³ The flexibility in zeolite RHO offers an opportunity to introduce a high degree of catalytic selectivity by controlled cation siting at reaction temperatures.

The framework of RHO is composed of a body-centered cubic arrangement of truncated cubo-octahedra or α -cages linked via double 8-rings. X-Ray powder structural studies by McCusker and Baerlocher⁴ have shown that RHO undergoes an appreciable distortion and loss of symmetry upon dehydration. The hydrated, partially sodium-exchanged Na,Cs-RHO exhibits centrosymmetric $Im\bar{3}m$ symmetry; however, upon dehydration, a tetrahedral deformation of the α -cages occurs to give the noncentrosymmetric space group, $I\bar{4}3m$. This change in symmetry is directly related to a 2.3% decrease in the lattice parameter from 15.031(1) to 14.678(1)Å. These overall features were first elucidated by Robson and

coworkers.⁵ Their refinements of X-ray powder film data indicated the structure described above, which had been proposed as a hypothetical zeolite structure earlier by Meier and Kokotailo.⁶ Despite good refinements in the space group $Im\bar{3}m$, the final residuals remained high, so lowering of the symmetry was attempted. The most significant improvement resulted from use of the sub group $I\bar{4}3m$. However, the resulting bond lengths were chemically unreasonable.

McCusker⁷ studied the deformation of the RHO framework occurring upon deammoniation. The ammonium form, ideally $(NH_4)_{12}Al_{12}Si_{36}O_{96}$, has a structure with $a = 14.821(1)\text{\AA}$ while in the hydrogen form, the framework shows little if any deviation from the ideal $Im\bar{3}m$ symmetry even at 500°C . Parise and co-workers⁸ found, from neutron powder refinements, on the hydrated (D_2O -RHO) form that the cell refined in the centrosymmetric space group with $a = 15.027(2)\text{\AA}$. The distortion of the dehydrated (D-RHO) form clearly showed a temperature dependence.⁹ At 11K, the cell refined in the noncentrosymmetric space group with a cell edge of about $14.601(1)\text{\AA}$. With increasing temperature the degree of the distortion of the cell decreased and finally disappeared above 800K.

Parise et al.¹⁰ defined a parameter, Δ , to describe the distortion or ellipticity of the double 8-ring whose major axes are orthogonal to each other. The effective cross-section of these rings and the size and shape of the openings connecting α -cages is related to Δ . For other zeolites, control over ring aperture dimensions is achieved typically using different sized cations as in zeolites 3A, 4A, and 5A. The cations K^+ , Na^+ , and Ca^{2+} in the A framework eclipse the ring opening to varying degrees depending on their

size and population. However, for zeolite RHO, it appeared to us that the framework itself could be used to modify the cage openings without actually blocking those openings.

Recently, we reported our initial observations describing the nature of framework distortions caused by cations in the absence of adsorbed molecular species.^{11,12} In the case of other cation- substituted zeolites, charge-compensation may produce lattice strain sufficient to promote decomposition of that zeolite under mild conditions.¹³ By virtue of its flexibility, the RHO framework is able to distort and relieve the strain imposed by the charge-compensating ions. We have therefore embarked on a systematic study of the effect of the charge compensating monovalent and divalent cations on the framework distortion of zeolite RHO.

Our earlier results suggested that the degree of distortion of the framework is related to the charge density of the cation. Partial reammoniation of H-RHO ($a = 15.1\text{\AA}$) yields a cell of 14.4245\AA . Even greater distortion of the cell is dependent on the specific monovalent ion-exchange; for example, Li,Cs-RHO and Ag-RHO produce cell edges of 14.4925\AA and 14.2251\AA , respectively.^{11,12} In this paper, we extend our studies to describe the effect of divalent ions and our results of *in situ* X-ray powder diffraction studies and structure refinement from neutron diffraction data of two divalent exchanged samples, Ca,ND₄-RHO and Ca,D-RHO.

EXPERIMENTAL

Ca,Cs-RHO. Na,Cs-RHO was prepared by a modification of the method described by Robson.¹⁴ Batches were prepared by adding 720 mL

of colloidal silica (Ludox[®] LS-30) to a mixture containing 200 mL 4 M Na₂AlO₂OH, 56 mL 50% CsOH, and 32 g NaOH in polytetrafluoroethylene (Teflon[®]) bottles, and allowed to stand at room temperature for 6 days. The resulting mixtures were heated at 100°C for 6 days and then filtered and thoroughly washed with distilled water. The dried powder was shown by X-ray powder diffraction to be highly crystalline zeolite RHO. Chemical analysis gave a unit cell composition of Na_{7.1}Cs_{3.8}Al_{11.5}Si_{36.5}O₉₆. Ten grams of this sample were ion exchanged by contacting the zeolite with 1L of a 1M solution of Ca(NO₃)₂ acidified with 9.6 mL of 0.1N HNO₃ for 7 days at room temperature. The resulting Ca,Cs-RHO zeolite was filtered and washed thoroughly with distilled water. Chemical analysis gave a unit cell composition of Ca_{3.4}Cs_{3.8}Na_{0.77}Al_{11.7}Si_{36.3}O₉₆.

Ca,NH₄-RHO. Na,Cs-RHO was first prepared and then exchanged six times (1 hour each) in aqueous 10% NH₄NO₃ (10 mL/g) at 90°C to give NH₄-RHO. The NH₄-RHO was exchanged twice (24 hours each) in aqueous 0.4M Ca(NO₃)₂ (10 mL/g) at 25°C. Then the sample was exchanged three additional times (24 hours each) in aqueous 0.4M Ca(NO₃)₂ (10 mL/g) at 90°C to give Ca,NH₄-RHO. Chemical analysis gave a unit cell composition of Ca_{4.0}(NH₄)_{3.3}Na_{0.13}Cs_{0.10}Al_{11.5}Si_{36.5}O₉₆ with NH₄ assumed from charge balance.

Ca-RHO. The NH₄-RHO as prepared above was exchanged six times (1 hour each) in aqueous 10% NaNO₃ (10 mL/g) at 90°C to give Na-RHO. The Na-RHO was exchanged six times (1 hour each) in aqueous 10% Ca(NO₃)₂ (10 mL/g) at 90°C to give Ca-RHO. Chemical analysis gave a unit cell composition of Ca_{5.8}Na_{0.70}Cs_{0.16}Al_{11.4}Si_{36.6}O₉₆.

Sr-RHO. Na-RHO, as prepared above, was exchanged six times (1 hour each) in aqueous 10% strontium acetate (10 mL/g) at 90°C. Chemical analysis gave a unit cell composition of $\text{Sr}_{5.2}\text{Na}_{0.10}\text{Cs}_{0.20}\text{Al}_{11.1}\text{Si}_{36.9}\text{O}_{96}$.

Ba-RHO. Na-RHO, as prepared above, was exchanged six times (1 hour each) in aqueous 10% $\text{Ba}(\text{NO}_3)_2$ (10 mL/g) at 90°C. Chemical analysis gave a unit cell composition of $\text{Ba}_{5.0}\text{Na}_{0.10}\text{Cs}_{0.23}\text{Al}_{11.0}\text{Si}_{37.0}\text{O}_{96}$.

Cd-RHO. Na-RHO, as prepared above, was exchanged six times (1 hour each) in aqueous 10% $\text{Cd}(\text{NO}_3)_2$ (10 mL/g) at 90°C. Chemical analysis gave a unit cell composition of $\text{Cd}_{4.8}\text{Na}_{0.06}\text{Cs}_{0.22}\text{Al}_{11.0}\text{Si}_{37.0}\text{O}_{96}$.

In situ X-ray powder diffraction studies of thermally and chemically induced transformations were monitored with a totally automated diffractometer-microreactor system.¹⁵ The equipment was designed for in situ structural studies of gas/liquid/solid and solid/solid interactions in the interval of 0 to 1000°C. The theta-theta vertical mode goniometer was automated for angular slew and step control, with on-line data collection and conversion for device display, and data transmission through network protocol. Reactor chamber temperature and precursor partial pressure were tailored to multiple-segment scans through an assemblage of microprocessors connected to six mass flow controllers. Phase transitions were surveyed as non-kinetic events through sequential inert gas sweep to 200 mL/min or sample chamber evacuation to 1 millitorr, either at controlled thermal ramp (°C/min/deg 2 θ) or isothermal set-point to 1000°C. For Ca,Cs- and Ca,NH₄-RHO, the samples were dehydrated at 80°C for 16 hours, followed by 2-hour hold and 2-hour X-ray scan sequences in increments of 50°C between 100°C and 500°C. The cooling cycle was executed in 100°C intervals to room

temperature, each two hours in duration for hold and scan. Ca-RHO was run in 2-minute ramp and 2-hour hold and scan sequences in increments of 100°C to 500°C and down, to room temperature.

Individual ASCII data files of 8000 steps (fixed time) per segment were ordered in 1 to 32 segments per setup file; multiple setups were utilized in each data collection run, that is, desorption under vacuum to the limit of temperature, sorption under controlled partial pressures of helium or ammonia or water to T_{max} , and subsequent desorption in time-dependent ramp-and-hold thermal cycles.

Cell parameters were refined using a modified least squares program after correcting sample peak locations through silicon internal standard thermal expansion reference positions. Generally, the range of refinement in two-theta was limited to 15 to 60°, because of unpredictable systematic errors below the first standard position. Full set refinement acceptance was based on the absence of systematic errors of magnitude exceeding two goniometer steps between approximately 10 and 60° two-theta, and rejection of any reflections whose calculated and observed (refined) difference exceeded two goniometer steps. Thus, unit cell dimensions are reported with errors at two standard deviations and are without discernable systematic errors under the conditions of the experiment. In instances where two phases were evident at or near the transition temperature, only a single set of standard lines was observed as evidence of sample flatness being maintained over the course of the transition and, ultimately, the experiment.

Point-to-point temperature differences across the length of the one inch square sample preparation did not exceed reported uncertainties of

types R, J, and K thermocouples at 500°C (approximately 3°) as monitored by three thermocouples positioned along the sample diagonal.

Deuterated forms (Ca,ND₄-RHO and Ca,D-RHO) were prepared for neutron powder diffraction study as follows.

Ca,ND₄-RHO. A sample of Ca,NH₄-RHO was loaded into a vacuum tight cell, attached to a manifold and evacuated while being heated to 250°C. The sample was kept under vacuum at that temperature for approximately 112 hours at which time, the sample was subjected to 3 D₂O exposures at 6 torr and pumped out to approximately 50 mtorr between exposures. After the final exposure, the sample was evacuated at 250°C for 32 hours and then sealed off.

Ca,D-RHO. A sample of Ca,NH₄-RHO was loaded into a vacuum tight cell, attached to a manifold and evacuated while being heated to 400°C. The sample was kept under vacuum at that temperature for approximately 112 hours and then cooled to 250°C. At 250°C, the sample was subjected to 3 D₂O exposures at 6 torr and pumped out to approximately 50 mtorr between exposures. After the final exposure, the sample was evacuated at 250°C for 16 hours after which it was again brought to 400°C under vacuum for an additional 16 h and then sealed off.

Room temperature neutron powder diffraction data were collected on the samples on diffractometer H4S at the High-Flux Beam Reactor, Brookhaven National Laboratory. Structural refinements were carried out using the program G.S.A.S.¹⁶ and in all cases framework-atom, bond-

distance, and angle restraints¹⁷ were used throughout the refinement.

TGA/MS was used to monitor water and ammonia desorption for the ammonium samples using a Du Pont 951 Thermal Gravimetric Analyzer interfaced to a Hewlett Packard 5970 Series Mass Spectrometer.

RESULTS AND DISCUSSION

The approach used in this study was to first examine the temperature dependence of the structural changes of the Cs,Cs-, Ca,NH₄-, Ca-, Sr-, Ba-, and Cd-RHO samples by in situ X-ray diffraction methods. Deammoniation and dehydration were monitored by TGA/MS under the same environmental conditions. Those materials which showed the greatest deviation from Im3m symmetry (smallest cell parameters) under similar thermal ramp-and-hold collection strategies were subsequently used for detailed structural analysis on deuterated samples upon data collection at B. N. L.

Examples of the powder diffraction patterns resulting from the in situ X-ray diffraction studies of the vacuum dehydration are given in Figures 1 (Ca,NH₄-RHO) and 2 (Cd-RHO). (Sequences of X-ray diffraction patterns for Ca,Cs-RHO, Ca-RHO, Sr-RHO, and Ba-RHO are available as supplementary material.) The variations in the different unit cell dimensions (Ca,Cs-, Ca,NH₄-, Ca-, Sr-, Ba-, and Cd-RHO) are illustrated in Figures 3A - 3F. The refined unit cell dimensions are given in Table I. The Ca-exchanged samples of zeolite RHO are unique in a number of respects with the smallest known unit cells for zeolite RHO, and for this reason are discussed below in detail.

Upon heating in vacuum to 50°C, the Ca,Cs-RHO sample loses water

and the cell contracts from about 15.0Å to 14.6Å (see Figure 3A). Unlike most of the previously studied systems of the ion-exchanged RHO^{11,12}, further heating to 500°C leads to contraction of the cell to about 14.34Å. Upon cooling to room temperature, the cell expands to about 14.5Å. This unusual behavior prompted us to examine the effect of calcium (in the absence of cesium) on the framework of zeolite RHO. The unit cell of Ca,NH₄-RHO (see Figures 1 and 3B) contracts from 14.45Å to about 14.0Å, at 250°C, the smallest cell edge yet observed for zeolite RHO. Upon cooling, the cell expands at 100°C and then contracts on reaching room temperature. A TGA/MS investigation on the original Ca,NH₄-RHO sample revealed two major events during heating. One centered at approximately 100°C corresponds primarily to sample dehydration/deammoniation and another centered at 400°C corresponds to the evolution of ammonia. This second event may be related to the anomalous cell expansion observed upon heating to 400°C in the *in situ* X-ray diffraction experiment. Finally, *in situ* X-ray diffraction studies of the Ca-RHO sample (see Figure 3C) shows water loss above 200°C resulting in a reduction in unit cell size from 14.4 to 14.0Å.

The observation of these highly distorted cells provoked the question of the siting of the Ca²⁺ ions and the determination of the structure of Ca,ND₄-RHO from powder neutron diffraction experiments. At room temperature, two phases coexist in this sample as shown in Figure 4a which shows the final observed, calculated and difference profiles from a two-phase Rietveld analysis of the data. The phases are defined as phase 1 (high ND₄/low Ca, $a = 14.410(2)\text{\AA}$) and phase 2 (low ND₄/high Ca, $a = 14.110(1)\text{\AA}$) and refined atomic parameters and residuals for both phases are given in Table II with selected bond distances and angles in Table III. It was

not possible to resolve the relative ND_4/Ca occupancies for these phases as the ions are at the same extra-framework cation site located and refined at the center of the double eight-ring. The phase with the smaller unit cell dimension (phase 2) has the larger calcium content, which distorts the eight-ring ellipse more than the bulky univalent ND_4 cation (phase 1). It is interesting that cell edge of Phase 1 is close to that observed at 400°C on heating the $\text{Ca},\text{NH}_4\text{-RHO}$ in the *in situ* X-ray diffraction experiment. Data obtained for the two-phase sample after heating to 400°C , however, show that this sample is a single phase $\text{Ca},\text{D-RHO}$, resulting from deammoniation and a redistribution of the Ca^{2+} cations. The results of the refinement are given in Table IV with selected bond distances and angles in Table V. The corresponding observed, calculated and difference profiles are shown in Figure 4b.

The framework structure of the double 8-ring for $\text{Ca},\text{D-RHO}$ is illustrated in Figure 5. The calcium cations are located at the center of the orthogonal double eight-ring, tetrahedrally coordinated to four framework oxygen atoms ($\text{Ca-O} = 2.70(1)\text{\AA}$). This distorts the eight-rings into highly anisotropic ellipses, in which Δ , the difference of the the major and minor axes¹⁰, is significantly greater than anything yet observed (2.49\AA). Framework distortion is driven by the cation siting to determine the lowest energy state of an ion-exchanged zeolite. In calcium-exchanged zeolite A, the calcium ions are sited in a trigonal environment within the 6-rings of the α -cage.¹⁸ In $\text{Ca},\text{D-RHO}$, the calcium ions reside in a very unusual and strained tetrahedral environment. Upon removal of water, the cations must use whatever charge compensating coordination is available, and, in this case the flexibility of the framework provides a tetrahedral environment rather

than the trigonal site associated with the six-ring. The significant distortion of the RHO framework by the calcium ion attests to the strong interaction between the framework and the ion. The lack of degradation of the sample upon calcination to 500°C is additional evidence of the stability of the RHO framework imparted by its ability to distort. It should also be noted that Li⁺ cations in zeolite RHO can be used to control the 8-ring channel opening (Δ) without obstruction of the channel by the cation in contrast to the siting found for Ca²⁺.

The dependency of the Δ parameter on cell dimensions from 13.9645Å to 15.0976Å is shown in Figure 6 and Table VI. The data show an almost linear dependence from $a = 14.2$ to 14.7 Å with a shift to non-linearity outside that range. The new data obtained in this study present an unusual opportunity to examine structural trends and framework flexibility in aluminosilicate molecular sieves. The variation of the average T-O bond length ($\langle T-O \rangle$) versus cell edge is shown in Figure 7. Linear regression analysis of the data ($R^2 = 0.72$) in Table VI collected at room temperature (excluding hydrated samples) shows a systematic increase in $\langle T-O \rangle$ as the unit cell dimensions decrease. The average T-O-T bond angle ($\langle T-O-T \rangle$) systematically ($R^2 = 0.91$) decreases with cell edge (Figure 8). The correlation ($R^2 = 0.90$) of decreasing $\langle T-O-T \rangle$ bond angle with increasing $\langle T-O \rangle$ bond length shown in Figure 9 has been described previously by Gibbs and coworkers.¹⁹ For a decrease in Si-O-Si bond angle from 147° to 131°, a decrease of 0.03Å is predicted in the Si-O bond length. This agrees remarkably well with the observed structural variations in zeolite RHO. The importance of cation-framework coordination in generating T-O framework distortions has been noted previously in single crystal studies of the

mordenite and chabazite families.^{20,21} In Figure 10, the variation of $\langle \text{T-O} \rangle$ versus f_s ¹⁹, where f_s is equal to $1/(1-\sec(\langle \text{T-O-T} \rangle))$, is given. Although f_s neglects the cation coordination and thermal motion^{19,22}, good agreement ($R^2 = 0.88$) is obtained.

As noted by Gibbs et al.¹⁹, the potential surface for T-O-T bond distortions has a very broad minimum. As a consequence, DLS modeling can be easily directed to a variety of non-unique configurations in a structure as flexible as that of zeolite RHO, and in fact has little predictive value unless particularly well defined constraints are used. These constraints are best obtained from experimental observations such as those available over the wide range of zeolite RHO unit cells. With this limitation in mind, we have used the observed values of $\langle \text{T-O} \rangle$, T-O(1)-T, T-O(2)-T, and T-O(3)-T as determined by regression analysis to define constraints to predict by DLS if even smaller channel windows and cubic cells are accessible. DLS calculations were performed using the Oxford CRYSTALS system.²³ For progressively smaller values of the unit cell edge, an average T-O bond distance and a single average T-O-T bond angle were determined from the observed trends as plotted in Figures 7 and 8. The structural model was then optimized in space group $I \bar{4}3m$ using the bond and angle restraints as determined above, as well as the angles defining a regular TO_4 tetrahedron. No second-nearest-neighbor restraints were included in the refinements.

With these particular restraints, the refinements suggest that the limiting factor in unit-cell contraction and framework distortion is the O(2)-O(3) contact between adjacent tetrahedra. For $a = 13.8 \text{ \AA}$, this distance is 2.59 \AA , reducing to 2.54 \AA at $a = 13.4 \text{ \AA}$. None of the other distances and

angles appear overstrained. Of course, this contact could be relieved by a distortion which we have not modelled by the simple DLS refinement. It seems likely, from the diffraction results on Ca,D-RHO, that the most significant feature in determining framework distortion and hence unit-cell size will be the specific interaction of the extra-framework cation with the framework, which could outweigh simple framework-only repulsion terms and even smaller unit-cell sized RHOs might be prepared.

Indeed, it is clear (Figure 11) that the degree of the observed distortions in zeolite RHO is related to the ionic size and charge of the ion-exchanged cation. In effect, the RHO framework, via its lattice parameter, can be considered a molecular strain gage. The Δ parameter or cell edge appears to be an effective measure of the strength of interaction of the RHO framework (negatively charged) and the charge compensating cations. The limit of the distortion can therefore be tested experimentally using cations with larger charge/radius ratios, such as Mg^{2+} , Be^{2+} , or Al^{3+} . In fact, Be-RHO can be indexed as tetragonal with $a = b = 13.192(2)\text{\AA}$, $c = 9.268(1)\text{\AA}$. The ratio of $a:b$ is 1.423, so that a and b are approximately $\sqrt{2} \times c$. The details of this structure as well as those of the above and other multivalent cation substituted RHO zeolites are presently being determined in order to test the DLS results.

CONCLUSIONS

We have synthesized and determined unit cell constants of less than 14.5\AA for ten different ions (Cd, Na, Tl, ND_4 , Rb, Li, Ag, Ba, Sr, and Ca). These are the smallest reported unit cells of RHO. The cell dimensions refined for these samples of Ca^{2+} -exchanged zeolite RHO are the smallest

observed to date. This observation underscores the flexibility and the stability of the RHO framework whose distortion is a direct measure of the strength of interaction of the charge compensating cations. Thus, the framework of zeolite RHO can be manipulated from about 15.1Å to 13.965Å by suitable ion exchange and calcination procedures. At the atomic level, this is accomplished via the unusual utilization of tetrahedrally coordinated Ca^{2+} . This ability to modify the dimensions of the internal void volume of microporous materials is essential either for size and shape dependent sorption behavior or for the tailoring of catalysts for reactant, product or transition state specificity.

ACKNOWLEDGMENT

The authors acknowledge R. L. Harlow for helpful discussions, as well as support by the Division of Material Sciences, U.S. Department of Energy under Contract DE-AC02-76CH0016 (DEC) and the Office of Naval Research (GDS).

SUPPLEMENTARY MATERIAL AVAILABLE:

Sequences of X-ray diffraction patterns for Ca,Cs-RHO, Ca-RHO, Sr-RHO, and Ba-RHO (Figures 12A-B, 13A-B, 14A-B, and 15A-B) are available (8 pages). Ordering information is given on any current masthead.

REFERENCES

1. Fyfe, C. A.; Kennedy, G. J.; De Schutter, C. T.; Kokotailo, G. T. *J. Chem. Soc.* **1984**, 541-542; Fyfe, C. A.; Stobl, H.; Kokotailo, G. T.; Kennedy, G. J.; Barlow, G. F. *J. Amer. Chem. Soc.* **1988**, *110*, 3373-3380; Schlenker, J. L.; Pluth, J. J.; Smith, J. V. *Mat. Res. Bull.* **1979**, *14*, 751 and references therein.
2. Bennett, J. M.; Blackwell, C. S.; Cox, D. E., In 'Intrazeolite Chemistry', G. D. Stucky and F. G. Dwyer, Eds., American Chemical Society, Washington, D C, 1983; *Adv. Chem. Ser.* **218**, pp.143-158; Bennett, J. M.; Blackwell, C. S.; Cox, D. E. *J. Phys. Chem.* **1983**, *87*, 3783-3790; Hay, D. G.; Jaeger, H.; West, G. W. *J. Phys. Chem.* **1985**, *89*, 1070-1072.
3. Natrolite, which has a small kinetic channel diameter of 2.6Å which will admit molecules smaller than ammonia, also has large framework distortions. (see Baur, W. H.; Fischer, R. X.; Shannon, R. D. In 'Innovation in Zeolite Materials Science', P. J. Grobet et al, Eds., Elsevier Science: Amsterdam, 1988, pp. 281-292).
4. McCusker, L. B.; Baerlocher, C., In 'Proceedings of the Sixth International Zeolite Conference', D. Olson and A. Bisio, Eds., Butterworths, Guildford, Surry, UK, 1984, pp. 812-822.
5. Robson, H. E.; Shoemaker, D. P.; Ogilvie, R. A.; Manor, P. C. *Adv. Chem. Ser.* **1973**, *121*, 106.
6. Meier, W. M.; Kokotailo, G. T. *Z. Kristallogr.* **1965**, *121*, 211.
7. McCusker, L. B. *Zeolites* **1984**, *4*, 51-55.
8. Parise, J. B.; Gier, T. E.; Corbin, D. R.; Cox, D. E. *J. Phys. Chem.* **1984**, *88*, 1635-1640.
9. Parise, J. B.; Abrams, L.; Gier, T. E.; Corbin, D. R.; Jorgensen, J. D.; Prince, E. *J. Phys. Chem.* **1984**, *88*, 2303-2307.

10. Parise, J. B.; Prince, E. *Mat. Res. Bull.* 1983, 18, 841-852.
11. Corbin, D. R.; Stucky, G. D.; Eddy, M. M.; Prince, E. E.; Abrams, L.; Jones, G. A. "Abstracts of Papers", 193rd National Meeting of the American Chemical Society, Denver, Colorado, April 1987; American Chemical Society: Washington, D.C., 1987; INOR 300.
12. Corbin, D. R.; Eddy, M. M.; Stucky, G. D.; Parise, J. B.; Vega, A. J.; Jones, G. A.; Abrams, L.; Cox, D. E., manuscript in preparation; Stucky, G. D.; Eddy, M. M.; Corbin, D. R.; Abrams, L.; Jones, G. A.; Prince, E., presented in part at the American Crystallographic Association Meeting, McMaster University, Ontario, Canada, June 1986.
13. Lutz, W.; Fahlke, B.; Lohse, U.; Buelow, M.; Richter-Mendau, J. *J. Crystal Res. & Technol.* 1983, 18(4), 513-518.
14. Robson, H. E. U. S. Patent 3,720,753 (1973).
15. Jones, G. A., presented in part at the American Crystallographic Association Meeting, Stanford University, Palo Alto, CA, 1985; Jones, G. A., presented in part at the Thirteenth International Congress of Crystallography, Hamburg, FRG, 1984; Jones, G. A., presented in part at the FASS Meeting, Philadelphia, PA, 1982.
16. von Dreele, R. B.; Larsen, A. C. Los Alamos Report LAUR 86-748.
17. C. Baerlocher, In 'Proceedings of the Sixth International Zeolite Conference', D. Olson and A. Bisio, Eds., Butterworths, Guildford, Surrey, UK, 1984, pp. 823-833; J. Waser, *Acta Cryst.* 1963, 16, 1091.
18. Pluth, J. J.; Smith, J. V. *J. Am. Chem. Soc.* 1983, 105, 1192.
19. Gibbs, G. V.; Meagher, E. P.; Newton, M. D.; Swanson, D. K. *Structure and Bonding in Crystals* 1981, 1, 195-225.
20. Smith, J. V. *Mater. Res. Bull.* 1979, 14, 849-856; Schlenker, J. L.; Pluth, J. J.; Smith, J. V. *Mater. Res. Bull.* 1979, 14, 751-758.

21. Mortier, W. J. *Mater. Res. Bull.* 1977, 12, 103-108; Mortier, W. J.; Pluth, J. J.; Smith, J. V. *Mater. Res. Bull.* 1977, 12, 97-102; Mortier, W. J.; Pluth, J. J.; Smith, J. V. *Mater. Res. Bull.* 1977, 12, 241-250.
22. Liebau, F., "Structural Chemistry of Silicates - Structure, Bonding, and Classification", Springer-Verlag: Germany, 1985; Chapter 3.
23. Watkin, D. J.; Carruthers, J. R.; Betteridge, P. W. CRYSTALS User Guide, Chemical Crystallography Laboratory, Oxford University, 1985.
24. Baur, W. H.; Fischer, R. X.; Shannon, R. D. In 'Innovation in Zeolite Materials Science', P. J. Grobet et al, Eds., Elsevier Science: Amsterdam, 1988, pp. 281-292.
25. Fischer, R. X.; Baur, W. H.; Shannon, R. D.; Staley, R. H.; Vega, A. J.; Abrams, L.; Prince, E. *J. Phys. Chem.* 1986, 90, 4414.
26. Baur, W. H.; Bieniok, A.; Shannon, R. D.; Prince, E., manuscript in preparation.
27. Fischer, R. X.; Baur, W. H.; Shannon, R. D.; Staley, R. H.; Abrams, L.; Vega, A. J.; Jorgensen, J. D. *Acta Cryst.* 1988, B44, 321-334.
28. Baur, W. H.; Fischer, R. X.; Shannon, R. D.; Staley, R. H.; Vega, A. J.; Abrams, L.; Corbin, D. R.; Jorgensen, J. D. *Z. Kristallogr.* 1987, 179, 281-304.

Table IA. Refined Cell Parameters from In situ Vacuum Dehydration of
Ca,Cs-RHO

<u>Temperature (°C)*</u>	<u>a(Å)</u>
25U	14.981(5)
50U	14.599(3)
80U	14.585(4)
100U	14.568(3)
150U	14.562(3)
200U	14.592(4)
250U	14.546(5)
300U	14.529(4)
350U	14.482(7)
400U	14.379(4)
500U	14.338(5)
400D	14.344(4)
300D	14.497(4)
200D	14.536(3)
100D	14.533(3)
25D	14.522(3)

* U = Up cycle; D = Down cycle

Table IB. Refined Cell Parameters from In situ Vacuum Dehydration of
Ca,NH₄-RHO

<u>Temperature (°C)*</u>	<u>a(Å)</u>
25U	14.454(3)
80U	14.465(2)
100U	14.466(2)
150U	14.431(2)
200U	14.385(2)
250U	14.069(2)
300U	14.031(3)
350U	13.977(5)
400U	14.427(3)
450U	13.980(3)
500U	13.973(3)
450D	13.977(3)
400D	13.970(5)
350D	13.974(2)
300D	14.029(3)
200D	14.003(2)
100D	14.383(5)
25D	13.996(4)

* U = Up cycle; D = Down cycle

Table IC. Refined Cell Parameters from In situ Vacuum Dehydration of Ca-RHO

<u>Temperature (°C)*</u>	<u>a(Å)</u>
25U	14.465(2)
100U	14.455(2)
200U	14.028(2)
300U	13.995(2)
400U	13.985(2)
500U	13.991(3)
400D	13.984(2)
300D	13.986(3)
200D	14.431(2)
100D	14.434(2)
25D	14.438(3)

* U = Up cycle; D = Down cycle

Table ID. Refined Cell Parameters from In situ Vacuum Dehydration of Sr-RHO

<u>Temperature (°C)*</u>	<u>a(Å)</u>
25U	14.669(2)
60U	14.598(2)
100U	14.591(2)
150U	14.591(1)
200U	14.586(2)
250U	14.542(2)
300U	14.083(2)
350U	14.074(3)
400U	14.073(3)
450U	14.066(3)
500U	14.064(2)
450D	14.060(2)
400D	14.057(2)
350D	14.048(3)
300D	14.050(2)
250D	14.045(1)
200D	14.045(1)
150D	14.580(2)
100D	14.580(2)
60D	14.574(2)
25D	14.617(2)

* U = Up cycle; D = Down cycle

Table IE. Refined Cell Parameters from In situ Vacuum Dehydration of Ba-RHO

<u>Temperature (°C)*</u>	<u>a(Å)</u>
25U	14.769(2)
60U	14.727(1)
100U	14.712(2)
150U	14.706(1)
200U	14.222(1)
250U	14.217(1)
300U	14.215(1)
350U	14.213(1)
400U	14.216(2)
450U	14.214(2)
500U	14.223(1)
400D	14.204(3)
300D	14.2016(8)
200D	14.184(2)
100D	14.701(2)
60D	14.702(3)
25D	14.723(3)

* U = Up cycle; D = Down cycle

Table IF. Refined Cell Parameters from In situ Vacuum Dehydration of Cd-RHO

<u>Temperature (°C)*</u>	<u>a(Å)</u>
25U	14.988(2)
60U	14.504(3)
100U	14.652(4)
150U	14.656(3)
200U	14.656(1)
250U	14.634(2)
300U	14.546(4)
350U	14.488(3)
400U	14.495(2)
450U	15.013(2)
500U	15.008(4)
450D	15.013(3)
400D	15.021(2)
350D	15.021(2)
300D	14.540(3)
250D	14.630(3)
200D	14.646(1)
150D	14.655(2)
100D	14.636(3)
60D	14.515(2)
25D	14.962(5)

* U = Up cycle; D = Down cycle

TABLE II. Refined Atomic Parameters for Ca,ND₄-RHO

Space group I $\bar{4}3m$
(International Tables No. 217)

Phase 1

<u>Atom</u>	<u>x</u>	<u>y</u>	<u>z</u>	<u>U(iso)</u>	<u>Pop.</u>
T(1)	0.2728(12)	0.1205(12)	0.4266(14)	1.7(7)	48
O(1)	0.2181(14)	0.2181(14)	0.4046(26)	1.7(7)	24
O(2)	0.1261(17)	0.1261(17)	0.6182(20)	1.7(7)	24
O(3)	0.0370(14)	0.2029(15)	0.3924(15)	1.7(7)	48
N(1)	0.5	0.0	0.0	4.0#	4.1

$$a = 14.410(2)\text{\AA}$$

$$R_p^a = 9.1\%$$

$$R_{wp}^b = 11.5\%$$

$$\text{Scale} = 19700$$

Phase 2

<u>Atom</u>	<u>x</u>	<u>y</u>	<u>z</u>	<u>U(iso)</u>	<u>Pop.</u>
T(1)	0.2759(11)	0.1274(11)	0.4306(13)	1.7(5)	48
O(1)	0.2324(12)	0.2324(12)	0.4110(19)	1.7(5)	24
O(2)	0.1185(14)	0.1185(14)	0.6238(18)	1.7(7)	24
O(3)	0.0441(11)	0.2082(13)	0.3869(13)	1.7(7)	48
Ca(1)	0.5	0.0	0.0	4.0#	6

$$a = 14.110(1)\text{\AA}$$

$$R_p^a = 16.1\%$$

$$R_{wp}^b = 21.8\%$$

$$\text{Scale} = 10919$$

a. $R_p = \sum |y_{oi} - I/C \cdot y_{ci}| / \sum |y_{oi}|$

b. $R_{wp} = [\sum S_i w_i (y_{oi} - I/C \cdot y_{ci})^2 / \sum S_i w_i y_{oi}^2]^{1/2}$

Not refined

TABLE III. Selected Bond Lengths (Å) and Angles(°)^a for Ca,ND₄-RHO

Phase 1

T - O(1)	1.643(12)	O(1) - T - O(2)	110.7
- O(2)	1.643(12)	O(1) - T - O(3)	112.8
- O(3)	1.638(13)	O(1) - T - O(3)	105.9
- O(3)	1.646(12)	O(2) - T - O(3)	104.9
		O(2) - T - O(3)	112.9
N(1) - 4xO(3)	3.08(3)	O(2) - T - O(3)	109.8
T - O(1) - T	141.7		
T - O(2) - T	145.1	$\Delta^b = 1.92\text{\AA}$	
T - O(3) - T	127.8		

Phase 2

T - O(1)	1.627(14)	O(1) - T - O(2)	111.2
- O(2)	1.644(14)	O(1) - T - O(3)	106.6
- O(3)	1.630(15)	O(1) - T - O(3)	109.4
- O(3)	1.635(14)	O(2) - T - O(3)	107.4
		O(2) - T - O(3)	110.4
Ca(1) - 4xO(3)	2.94(4)	O(2) - T - O(3)	111.7
T - O(1) - T	131.1		
T - O(2) - T	132.3	$\Delta^b = 2.31\text{\AA}$	
T - O(3) - T	139.7		

a. Errors on bond angles are 1°.

b. The Δ parameter is defined in the text and in reference 10.

TABLE IV. Final Parameters for Ca,D-RHO

Space group I $\bar{4}3m$
(International Tables No. 217)

<u>Atom</u>	<u>x</u>	<u>y</u>	<u>z</u>	<u>U(iso)</u>	<u>Pop.</u>
T(1)	0.2816(10)	0.1310(10)	0.4345(10)	4.0(7)	48
O(1)	0.2365(7)	0.2365(7)	0.4141(8)	4.3(6)	24
O(2)	0.1104(7)	0.1104(7)	0.6142(9)	4.7(7)	24
O(3)	0.0481(6)	0.2032(7)	0.3913(7)	3.3(5)	48
Ca(1)	0.5	0.0	0.0	6.0#	3.4

$$a = 13.9645(7)\text{\AA}$$

$$R_p^a = 9.6\%$$

$$R_{wp}^b = 12.6\%$$

a. $R_p = \sum |y_{oi} - I/C \cdot y_{ci}| / \sum |y_{oi}|$

b. $R_{wp} = [\sum w_i (y_{oi} - I/C \cdot y_{ci})^2 / \sum w_i y_{oi}^2]^{1/2}$

Not refined

TABLE V. Selected Bond Lengths (Å) and Angles(°)^a for
Ca,D-RHO

T - O(1)	1.621(12)	O(1) - T - O(2)	115.0
- O(2)	1.649(13)	O(1) - T - O(3)	113.2
- O(3)	1.631(14)	O(1) - T - O(3)	107.2
- O(3)	1.704(14)	O(2) - T - O(3)	102.9
		O(2) - T - O(3)	110.9
Ca(1) - 4xO(2)	2.70(1)	O(2) - T - O(3)	107.3
T - O(1) - T	133.1		
T - O(2) - T	132.4	$\Delta^b = 2.49\text{\AA}$	
T - O(3) - T	130.2		

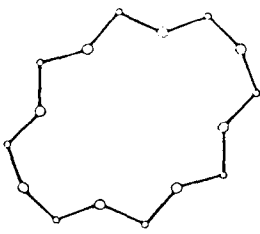
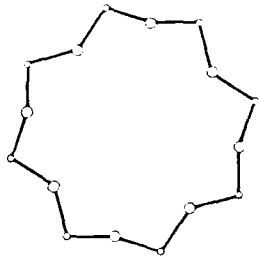
a. Errors on bond angles are 1°.

b. The Δ parameter is defined in the text and in reference 10.

Table VI. Summary of RHO Structural Data

Form	Temperature(K)	a(Å)	$\Delta(\text{\AA})$	$\langle \text{I} \cdot \text{O} \rangle$	$\langle \text{T-O-T} \rangle$	Reference	8-Ring Configuration
CaD	298	13.9645	2.49	1.651	131.5	a	
Sr	473	14.045				11,a	
CaND ₄ (II)	298	14.110	2.31	1.642	135.6	a	
Ba	473	14.184				11,a	
Ag	298	14.2251	2.21	1.649	133.4	11,12	
Li	298	14.3390				11,12	
LiND ₄	298	14.372				11,12	
Rb	298	14.375	2.08	1.648	136.5	12	
CaND ₄ (I)	298	14.410	1.92	1.642	135.6	a	
(ND ₄) ₆	11	14.4245	1.95	1.640	137.5	9,11,12	
(ND ₄) ₆	11	14.425	1.93	1.637	137.9	25	
Tl	298	14.461	1.96	1.644	138.9	12	
Na	298	14.4848				11,12	
Cd	623	14.488				11,a	
LiCs	298	14.4925	1.89	1.645	137.1	11,12	
(ND ₄) ₆	298	14.5264	1.84	1.631	140.7	24	
D	11	14.601	1.68	1.635	140.0	9	
K	298	14.613	1.69	1.648	136.5	12	
D	13	14.620				25	
CsD	298	14.6536	1.60	1.640	139.8	10	
NaCs(H ₂ O)	298	14.6566	1.57	1.636	140.8	24,26	
CsD	298	14.6652	1.57	1.638	140.8	10	

Table VI. Summary of RHO Structural Data Cont'd

Form	Temperature(K)	a(Å)	$\Delta(\text{\AA})$	$\langle T-O \rangle$	$\langle T-O-T \rangle$	Reference	8-Ring Configuration
NaCs	298	14.678	1.68	1.683	132.8	4	
dD	294	14.694	1.52	1.632	143.0	8	
CsD	493	14.7014	1.49	1.642	139.8	10	
D	295	14.7237	1.52	1.630	143.5	9	
K(H ₂ O)	298	14.7412				11	
D	423	14.7580	1.40	1.632	143.8	9	
(NH ₄) ₁₂	373	14.821	1.56	1.632	143.8	7	
D	13	14.850	0	1.610	145.8	25	
D	573	14.8680	1.14	1.645	141.0	9	
D	298	14.8803	1.17	1.632	144.5	27	
CD ₃ OD	11	14.969	0.84			9	
H	773	14.982	0	1.610	149.2	7	
Ca		14.995	0.29			9	
H	293	15.00	0	1.610	145.7	5	
D ₂ O	423	15.027	0	1.655	142.5	8	
NaCs(H ₂ O)	298	15.031	0	1.660	139.6	4	
D	298	15.0387	0	1.624	146.8	27	
D	623	15.0620	0	1.625	147.5	27	
D	298	15.0686	0	1.627	146.8	28	
D	298	15.0696	0	1.626	147.1	28	
D	623	15.0799	0	1.627	147.0	28	
D	298	15.0976	0	1.629	146.8	28	

a. This Work

FIGURE CAPTIONS

Figure 1. Sequence of X-ray powder diffraction patterns (Cu K α radiation, $\lambda = 1.5418\text{\AA}$) for Ca,NH₄-RHO: (a) Up cycle and (b) Down cycle.

Figure 2. Sequence of X-ray powder diffraction patterns (Cu K α radiation, $\lambda = 1.5418\text{\AA}$) for Cd-RHO: (a) Up cycle and (b) Down cycle.

Figure 3. Variation of cell dimension with temperature for (a) Ca,Cs-RHO, (b) Ca,NH₄-RHO, (c) Ca-RHO, (d) Sr-RHO, (e) Ba-RHO, and (f) Cd-RHO.

Figure 4. Final calculated (line) and observed (crosses) neutron powder diffraction profiles for (a) Ca,ND₄-RHO and (b) Ca,D-RHO. In each case, the difference pattern (observed minus calculated) is shown below on the same scale as the observed pattern. Tickmarks at the bottom line of the profile indicate peak positions.

Figure 5. The framework structure of the double 8-ring for Ca,D-RHO.

Figure 6. Scatter plot of cell edge (a) versus Δ .

Figure 7. Variation of cell edge (a) versus $\langle T-O \rangle$ (filled squares - room temperature data (excluding hydrated samples)); filled triangles - all data.

Figure 8. Variation of cell edge (a) versus $\langle T-O-T \rangle$ (filled squares - room temperature data (excluding hydrated samples)); filled triangles - all data.

Figure 9. Variation of $\langle T-O \rangle$ versus $\langle T-O-T \rangle$ (filled squares - room temperature data (excluding hydrated samples)); filled triangles - all data.

Figure 10. Variation of $\langle T-O \rangle$ versus f_s (filled squares - room temperature data (excluding hydrated samples)); filled triangles - all data.

Figure 11. Variation of cell edge (a) versus Z^2/r with Z = ionic charge and r = ionic radius.

FIGURE 1A

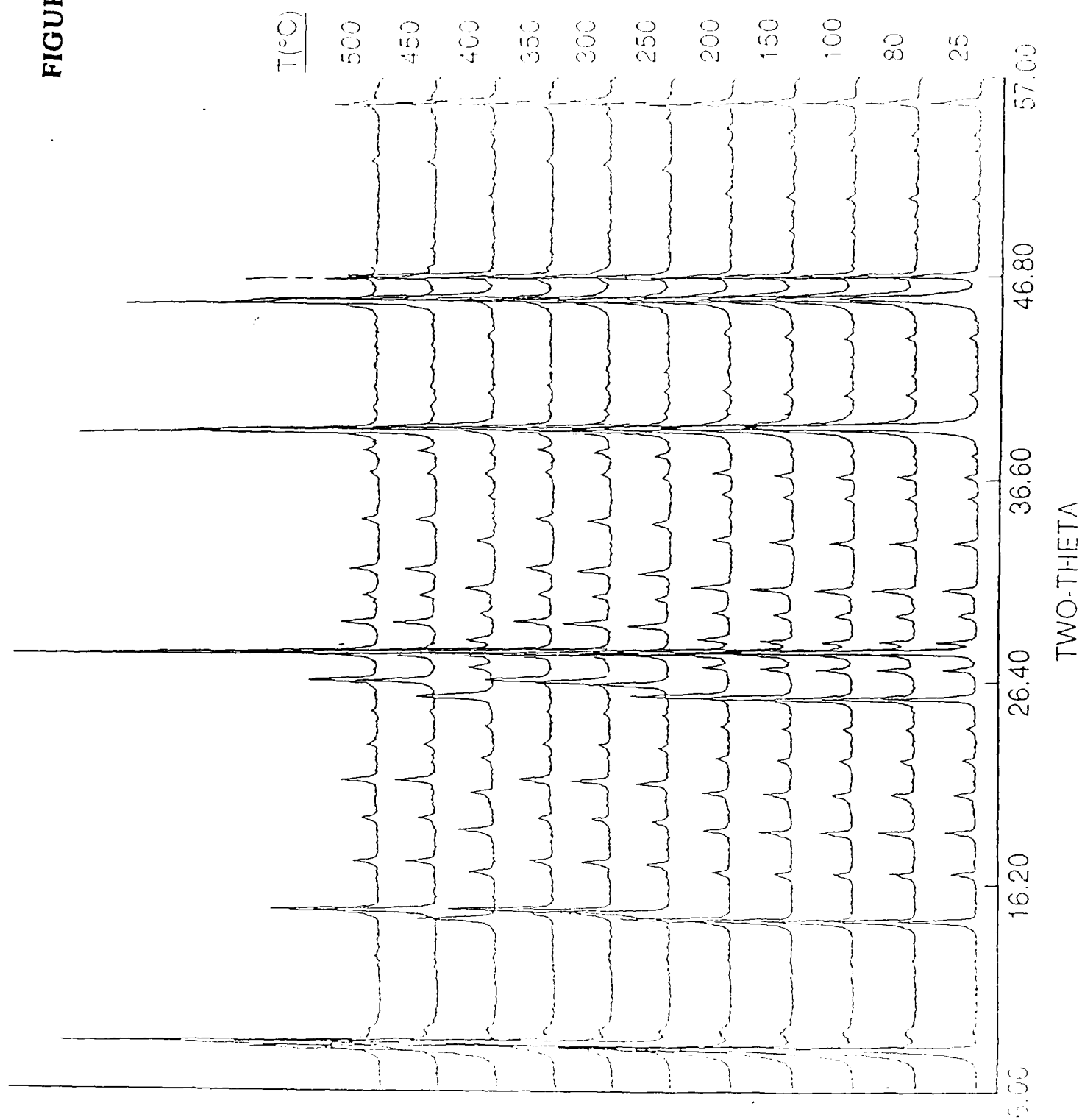


FIGURE 1B

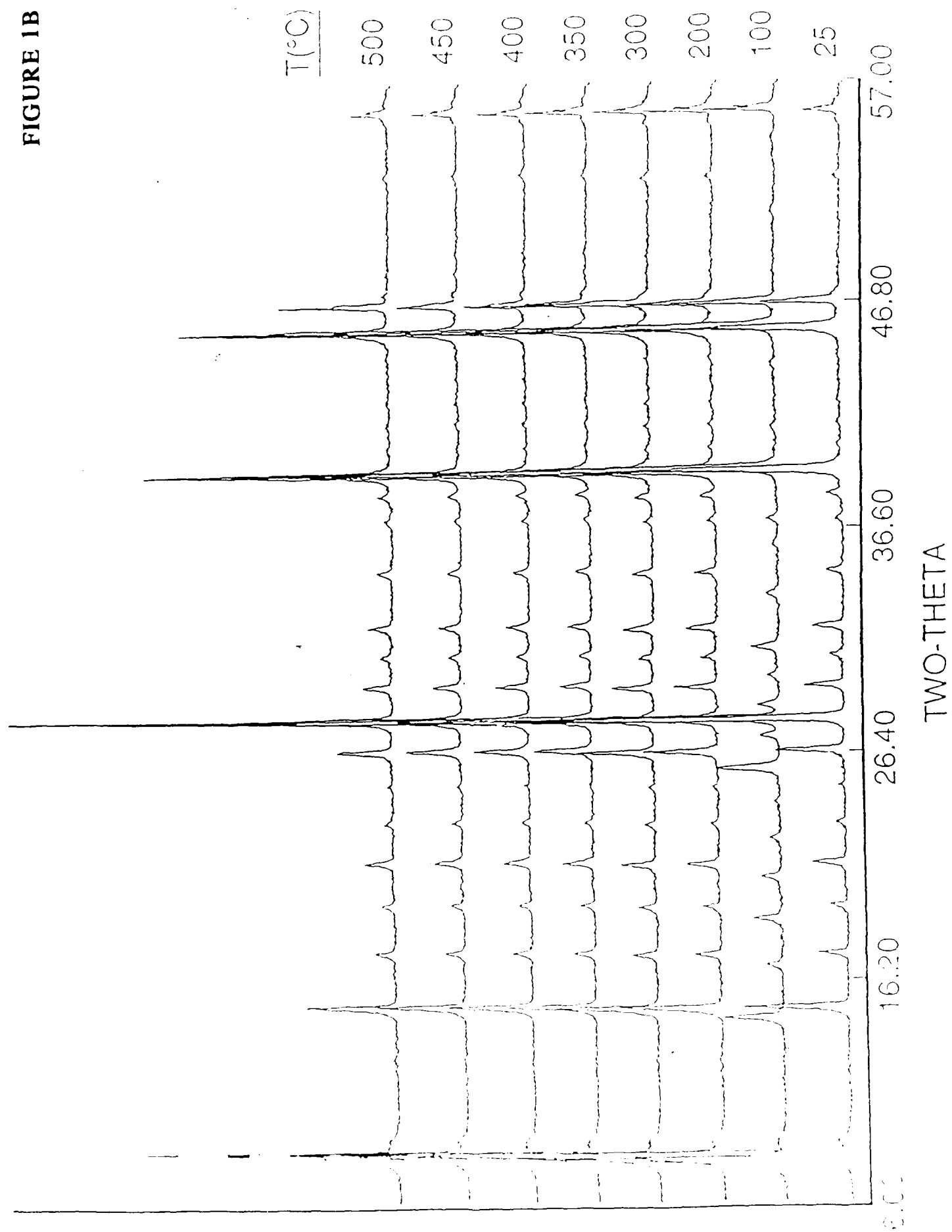


FIGURE 2A

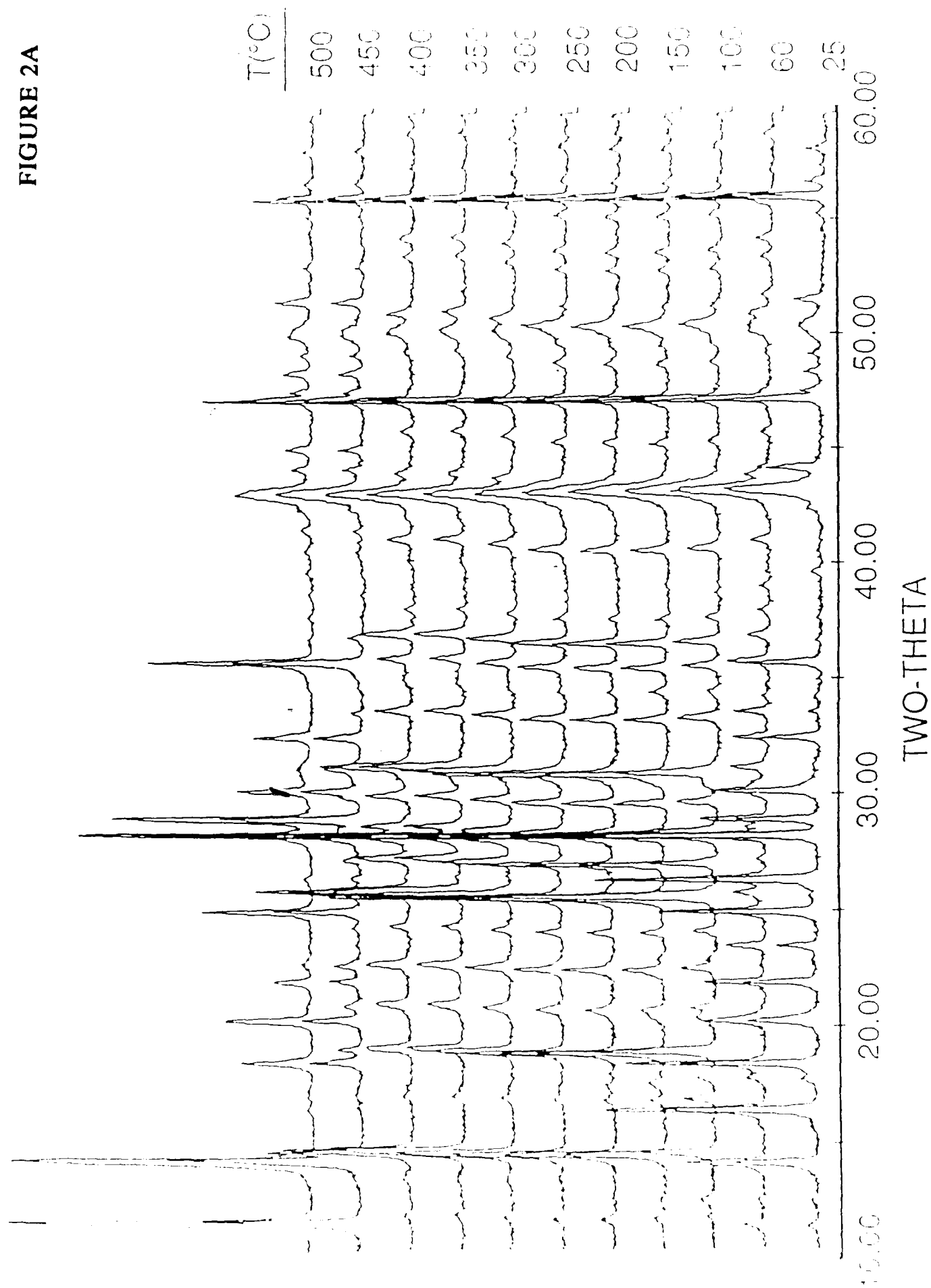


FIGURE 2B

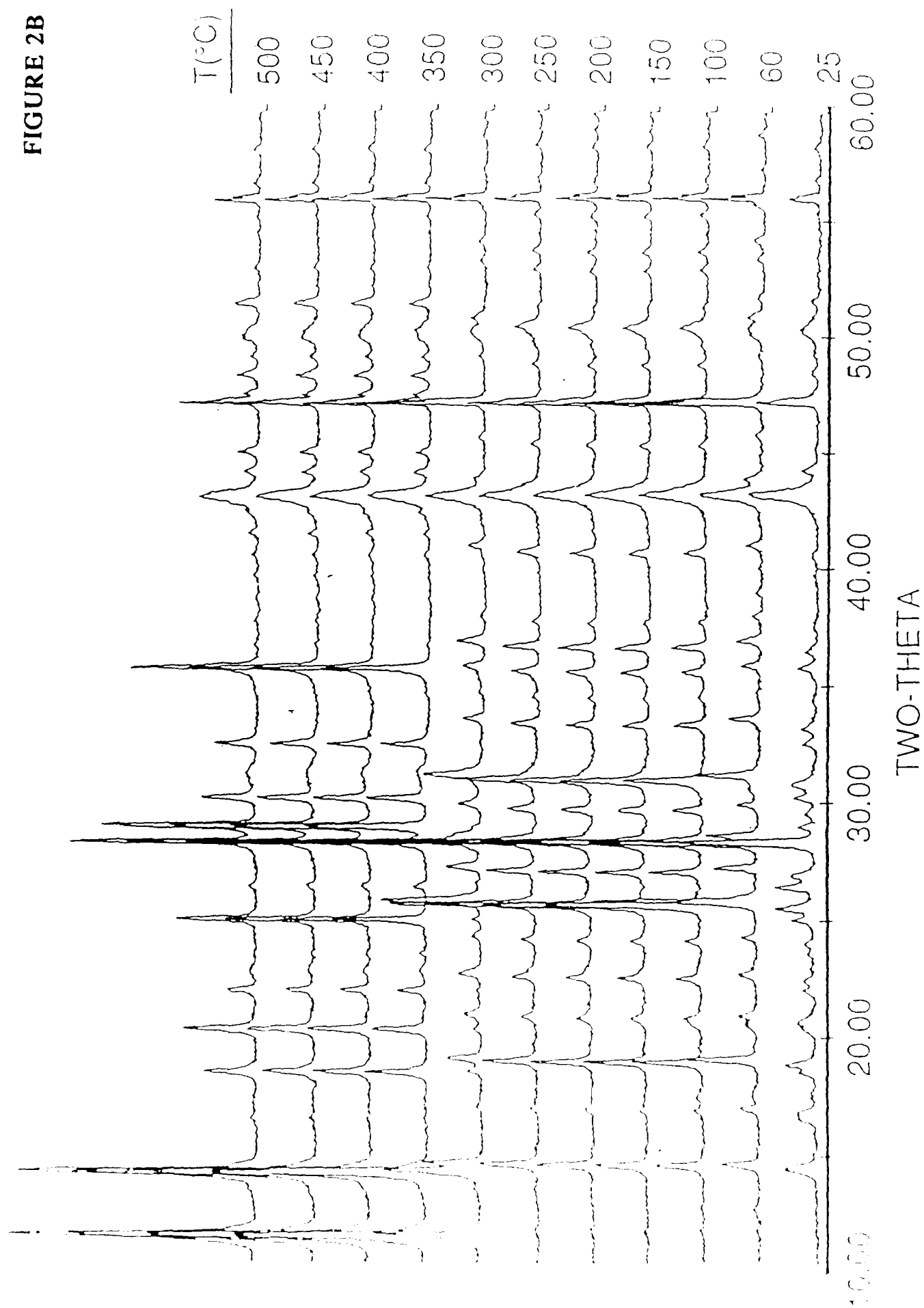


FIGURE 3-1

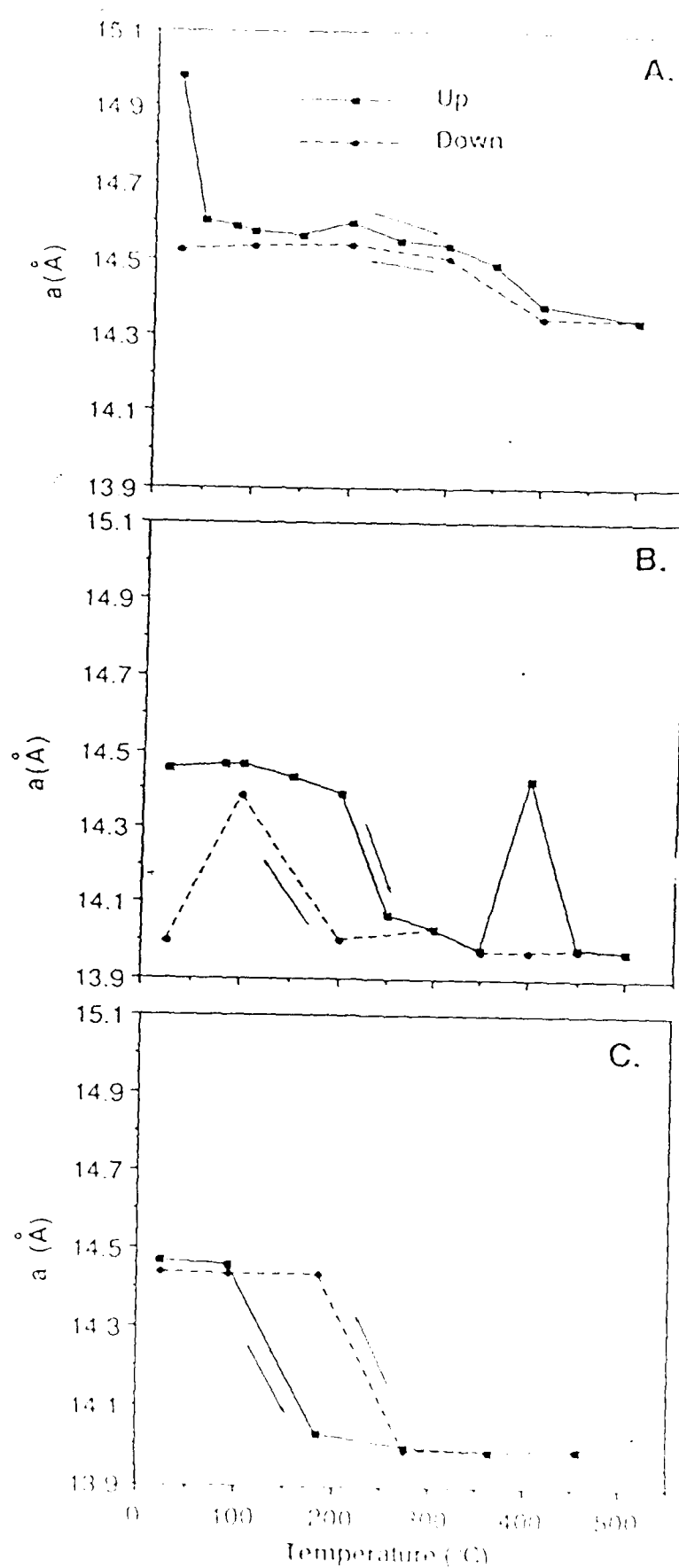


FIGURE 3-2

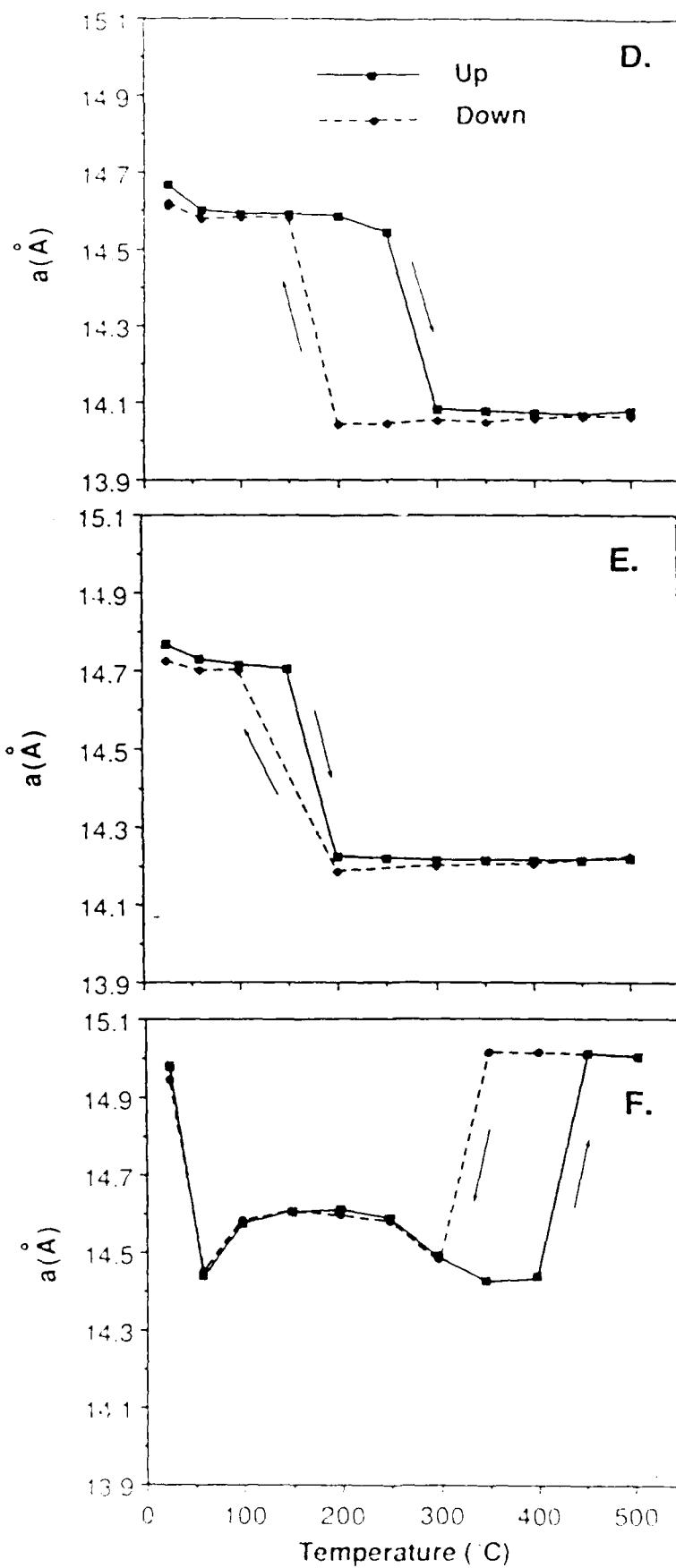


FIGURE 4A

LAMBDA 2.3700 A

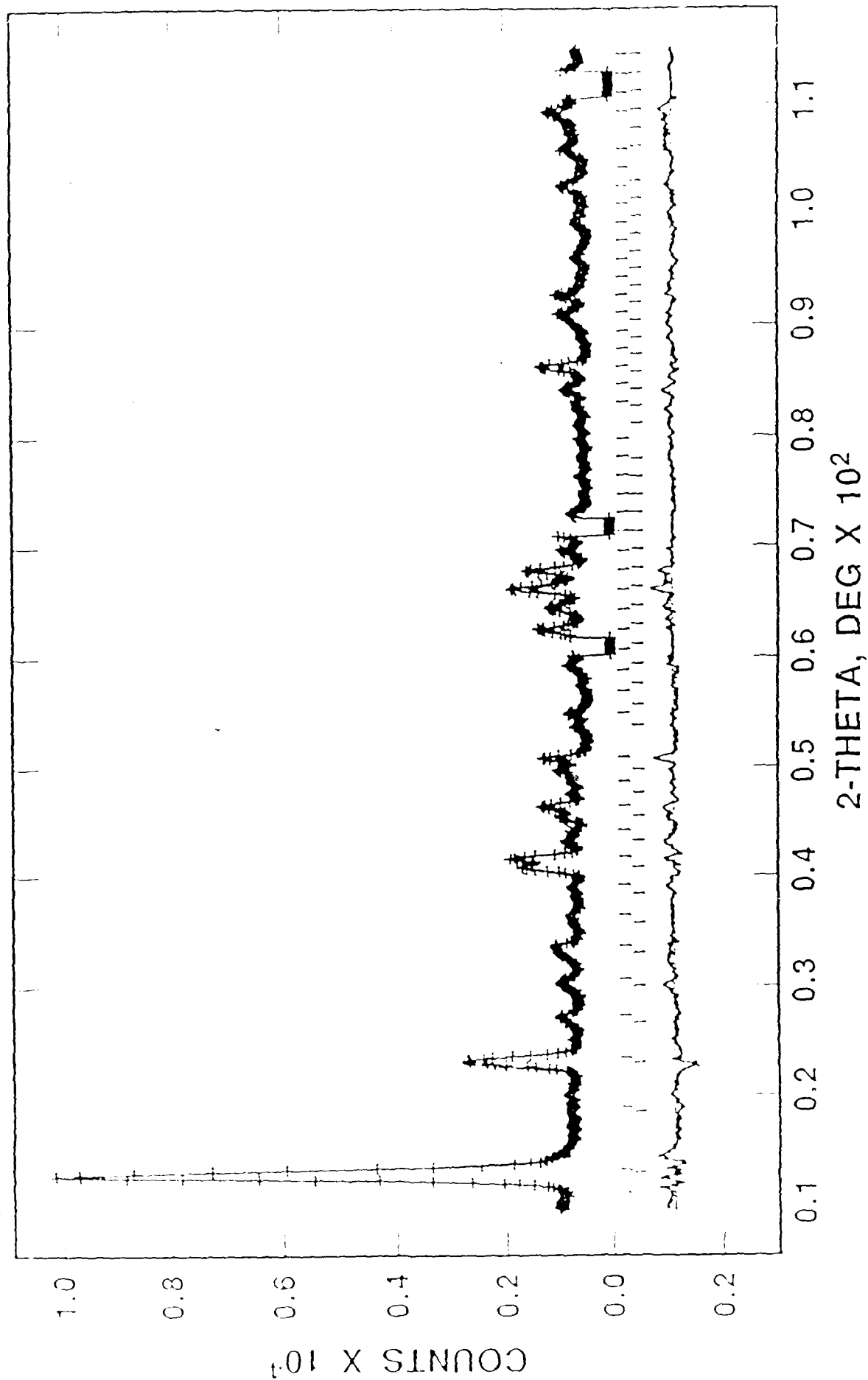


FIGURE 4B

LAMBDA 2.3700 A

OBSD. AND DIFF. PROFILES

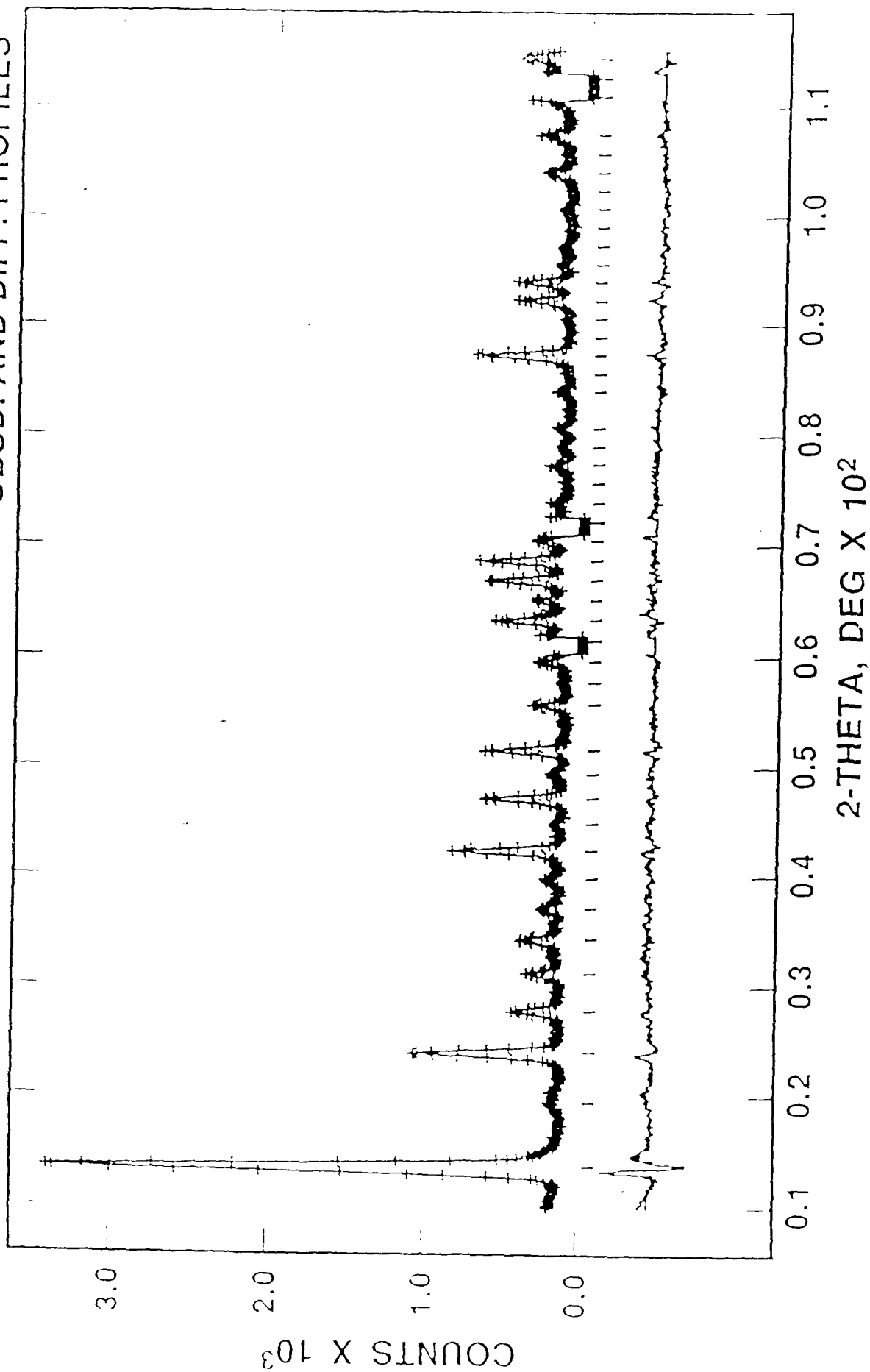


FIGURE 5

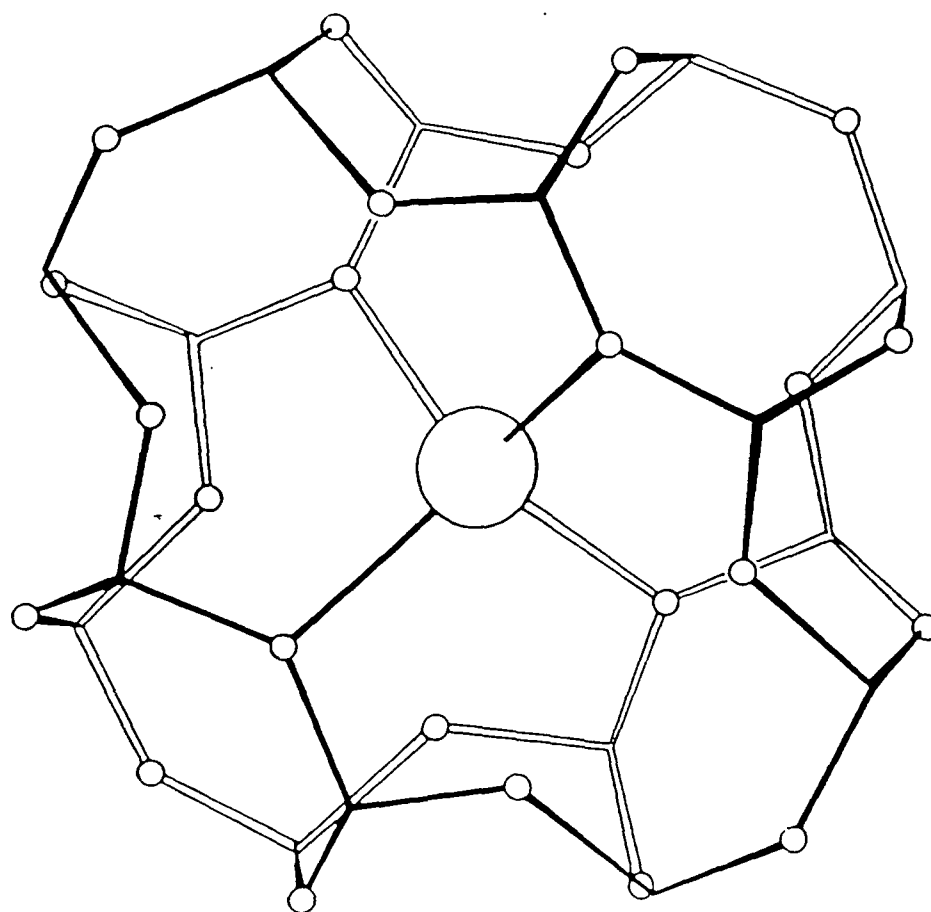


FIGURE 6

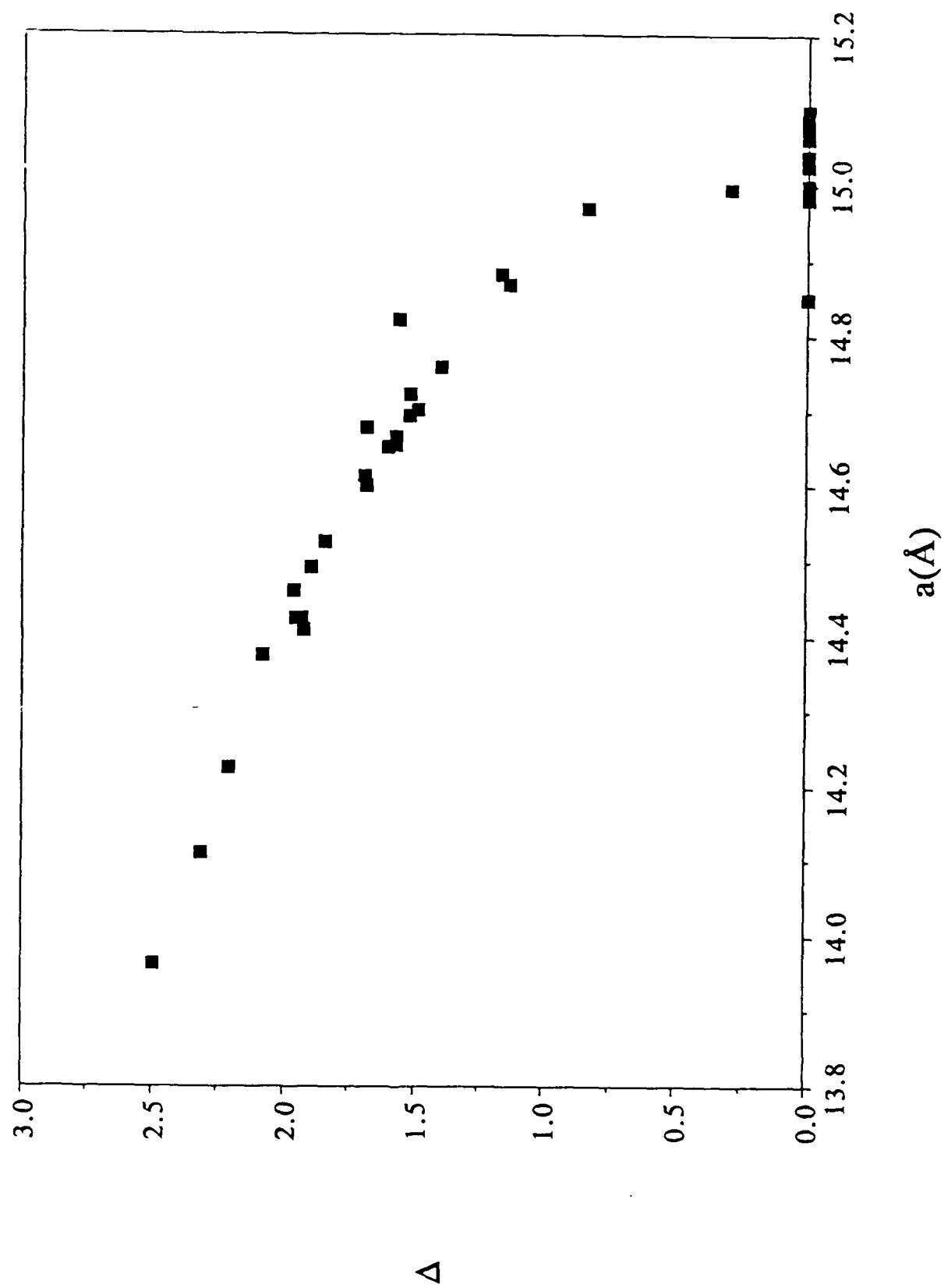


FIGURE 7

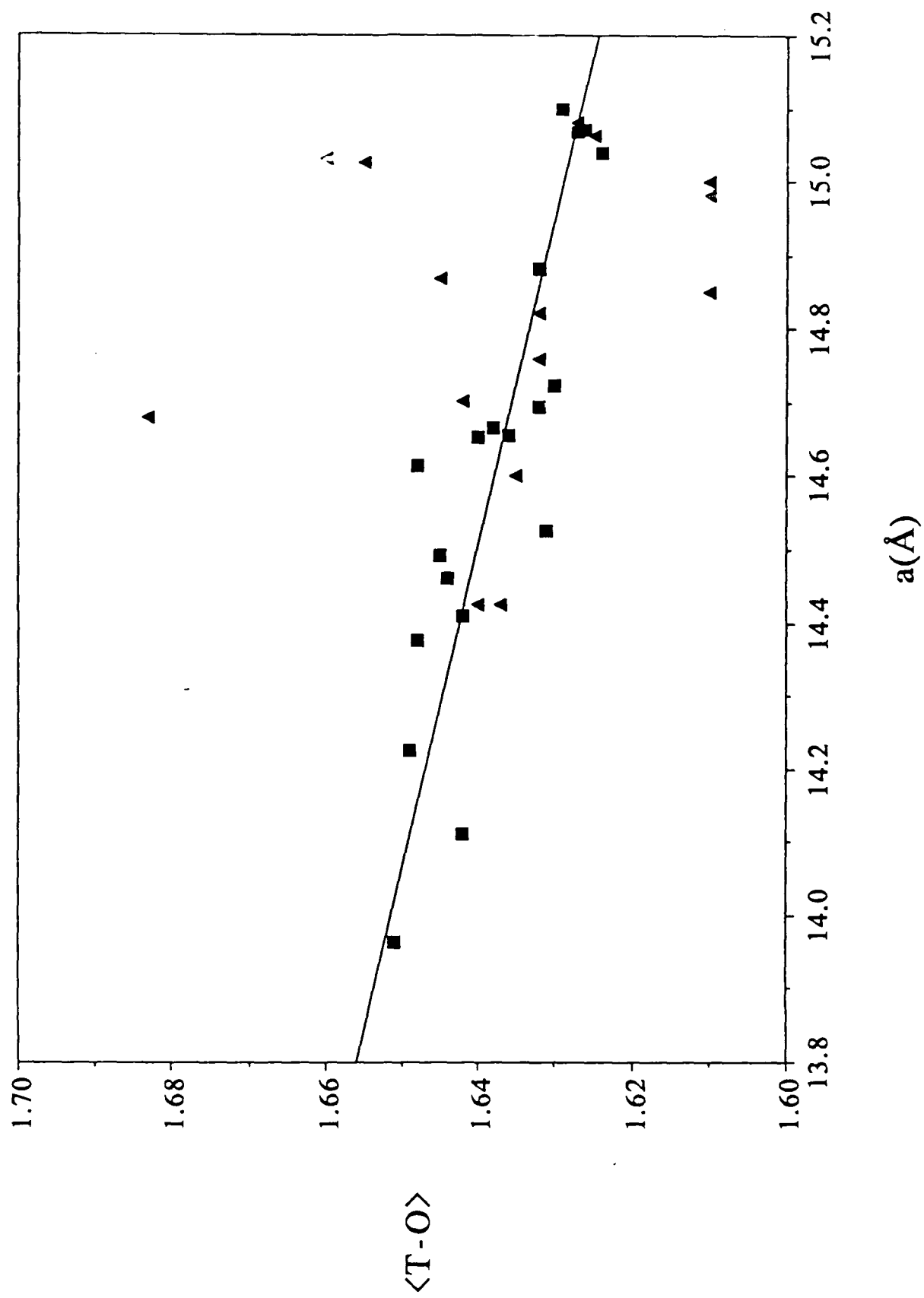


FIGURE 8

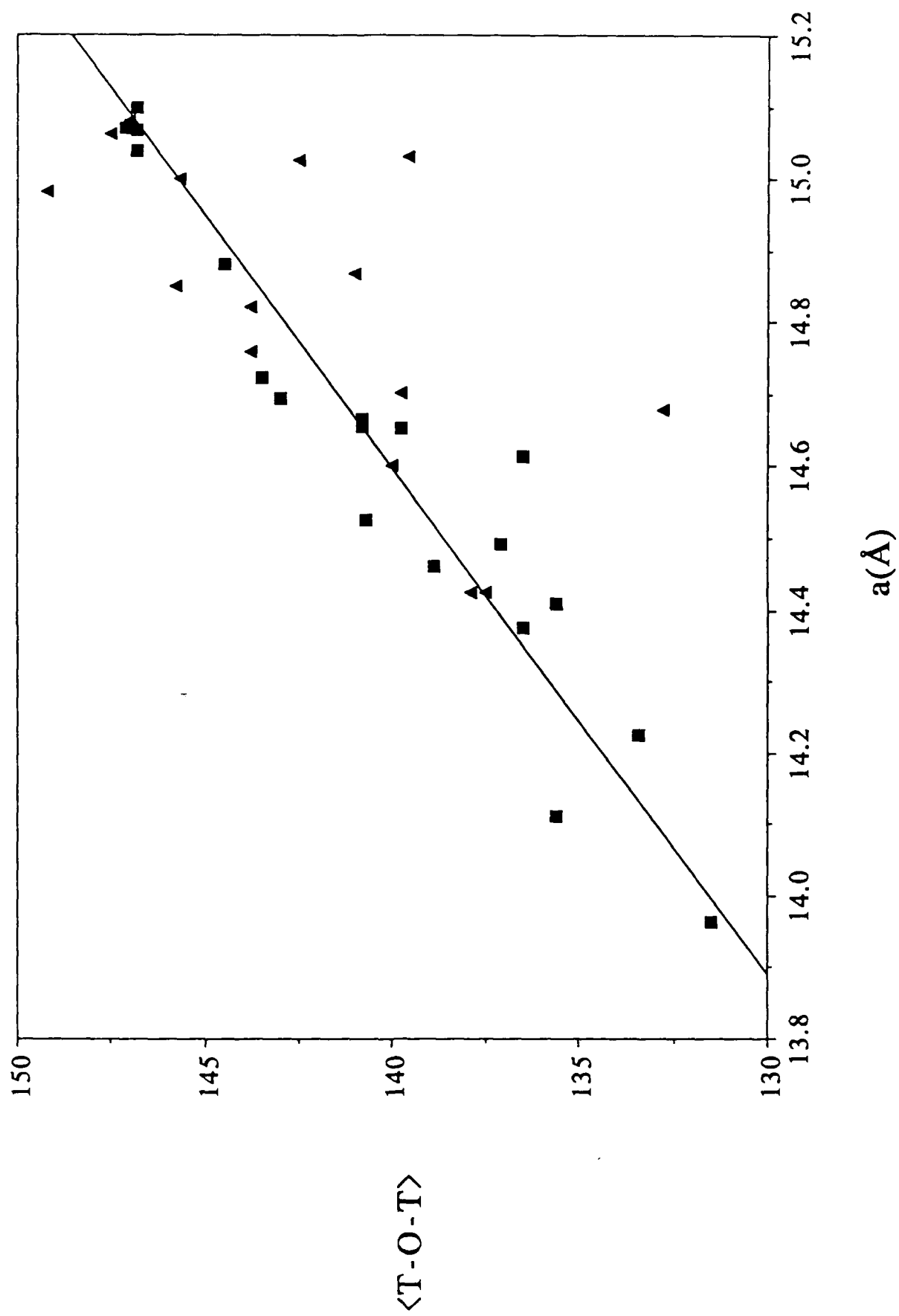


FIGURE 9

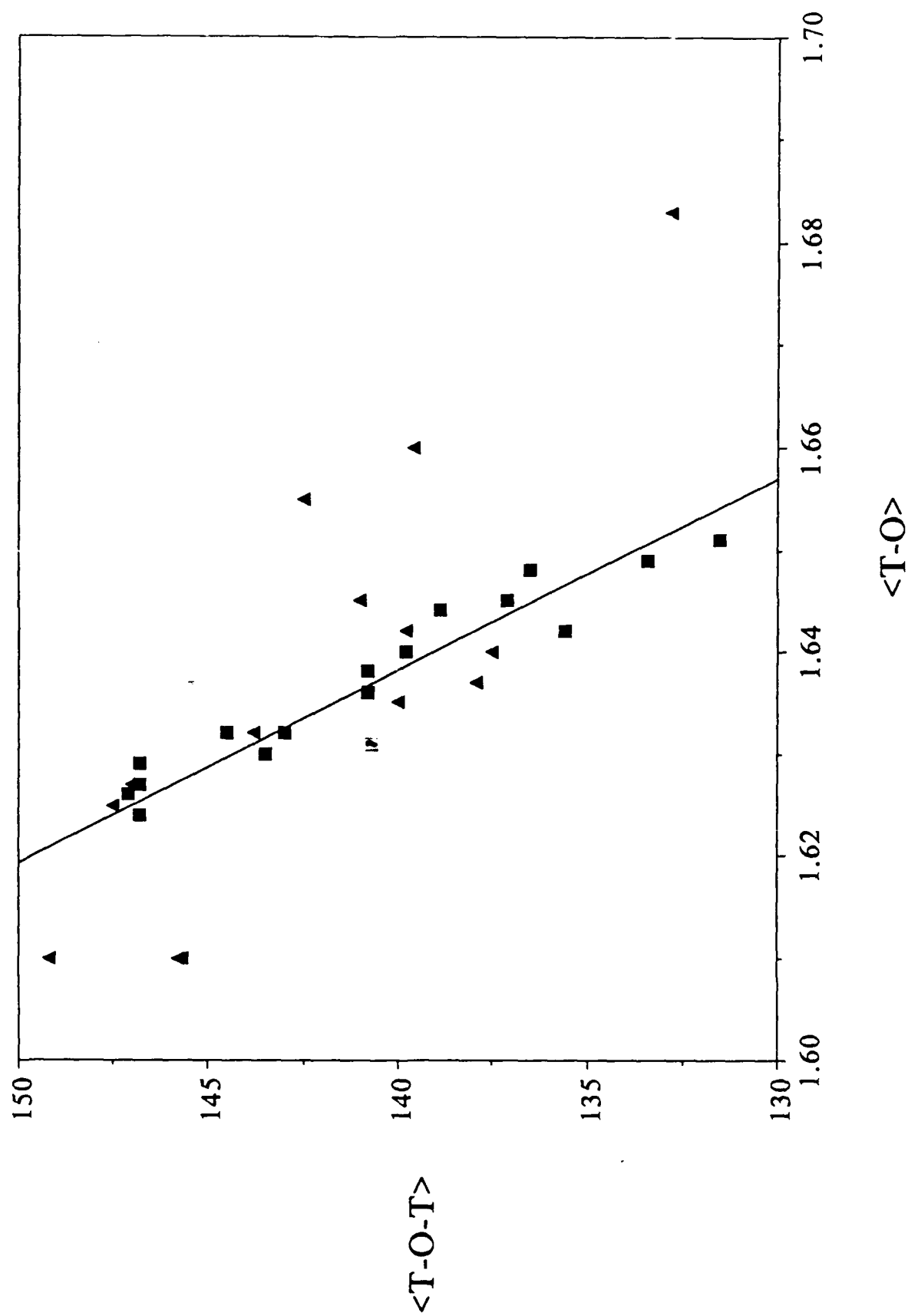


FIGURE 10

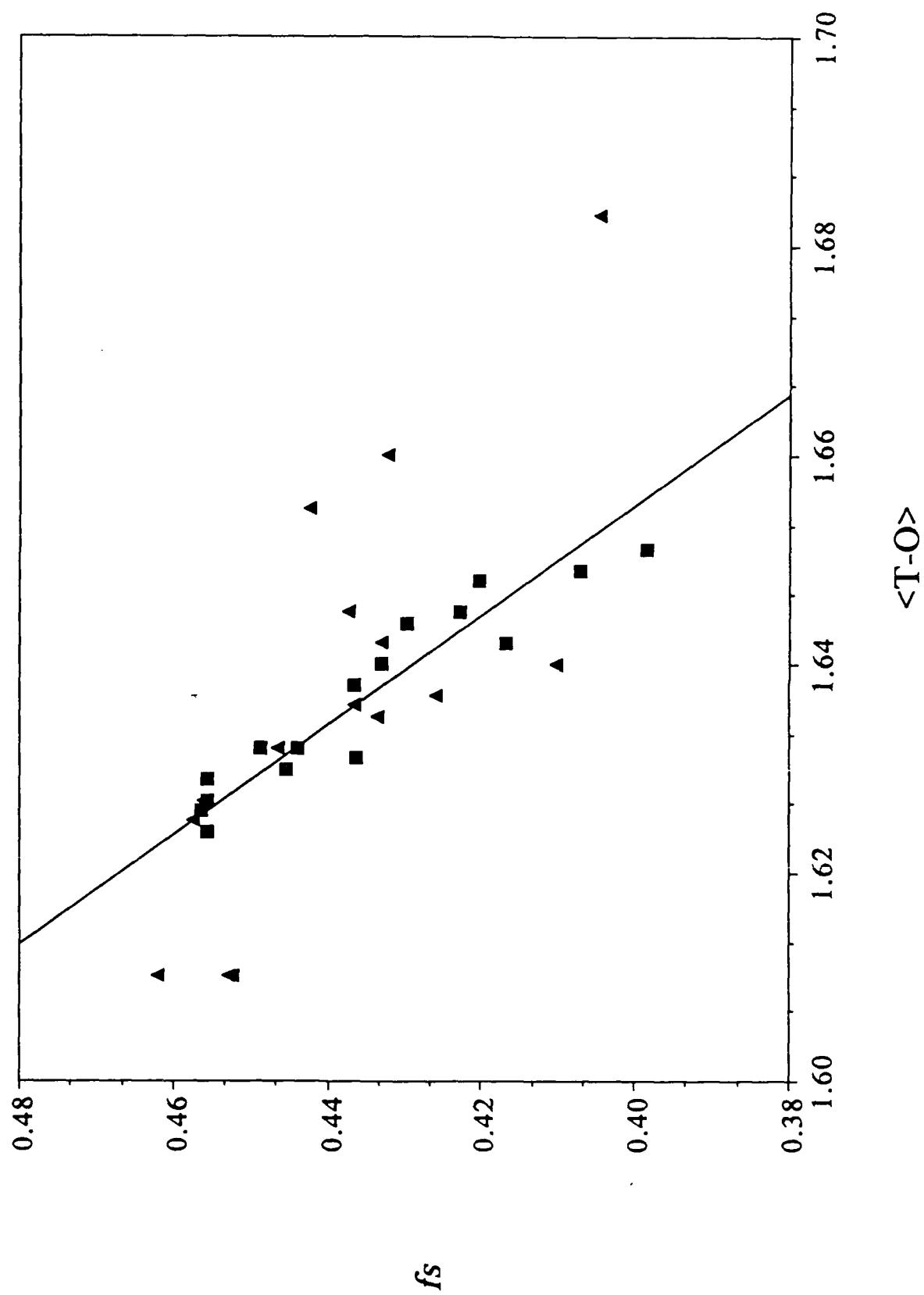
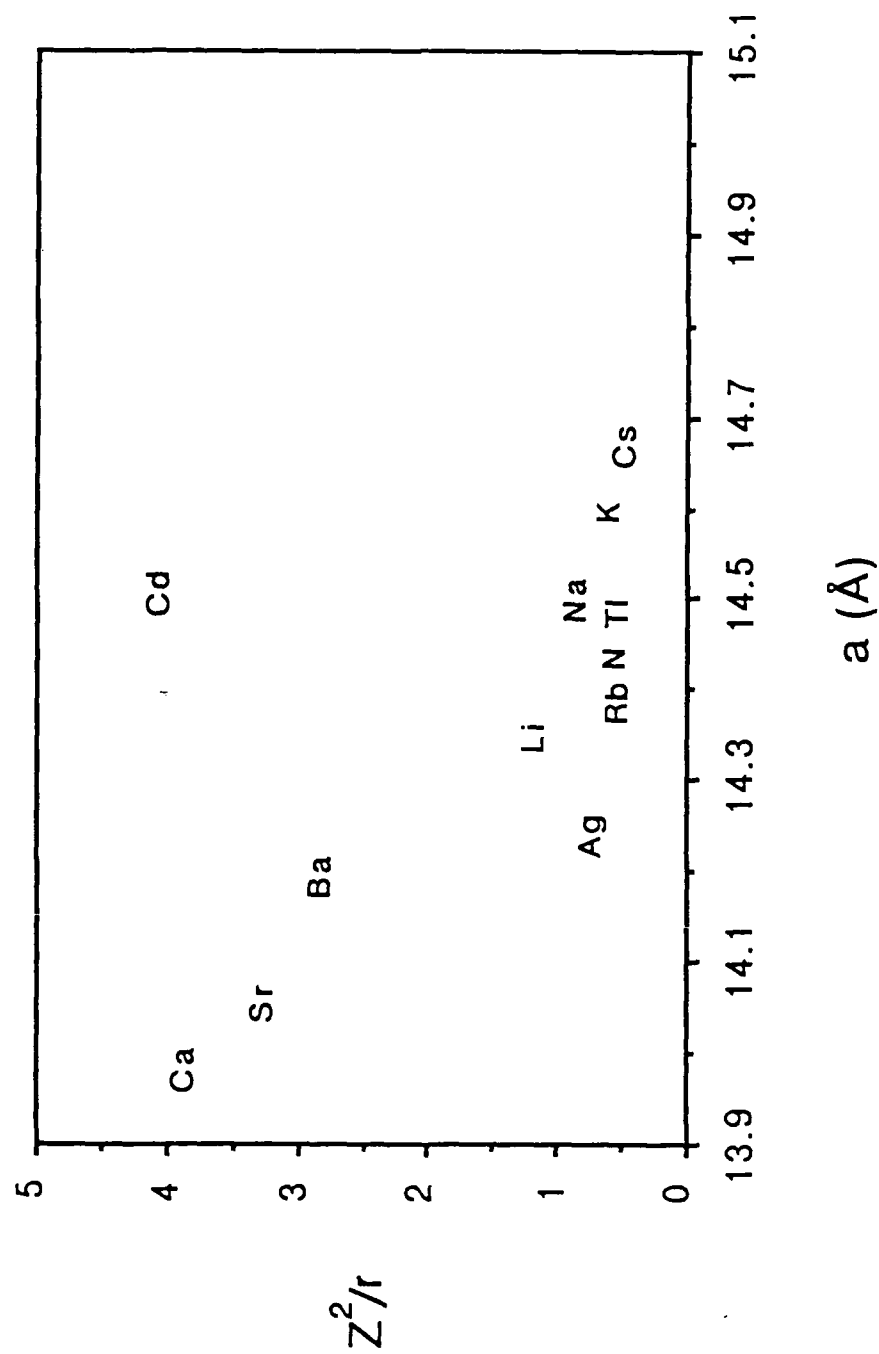


FIGURE 11



SUPPLEMENTARY MATERIAL

FIGURE 12A-1

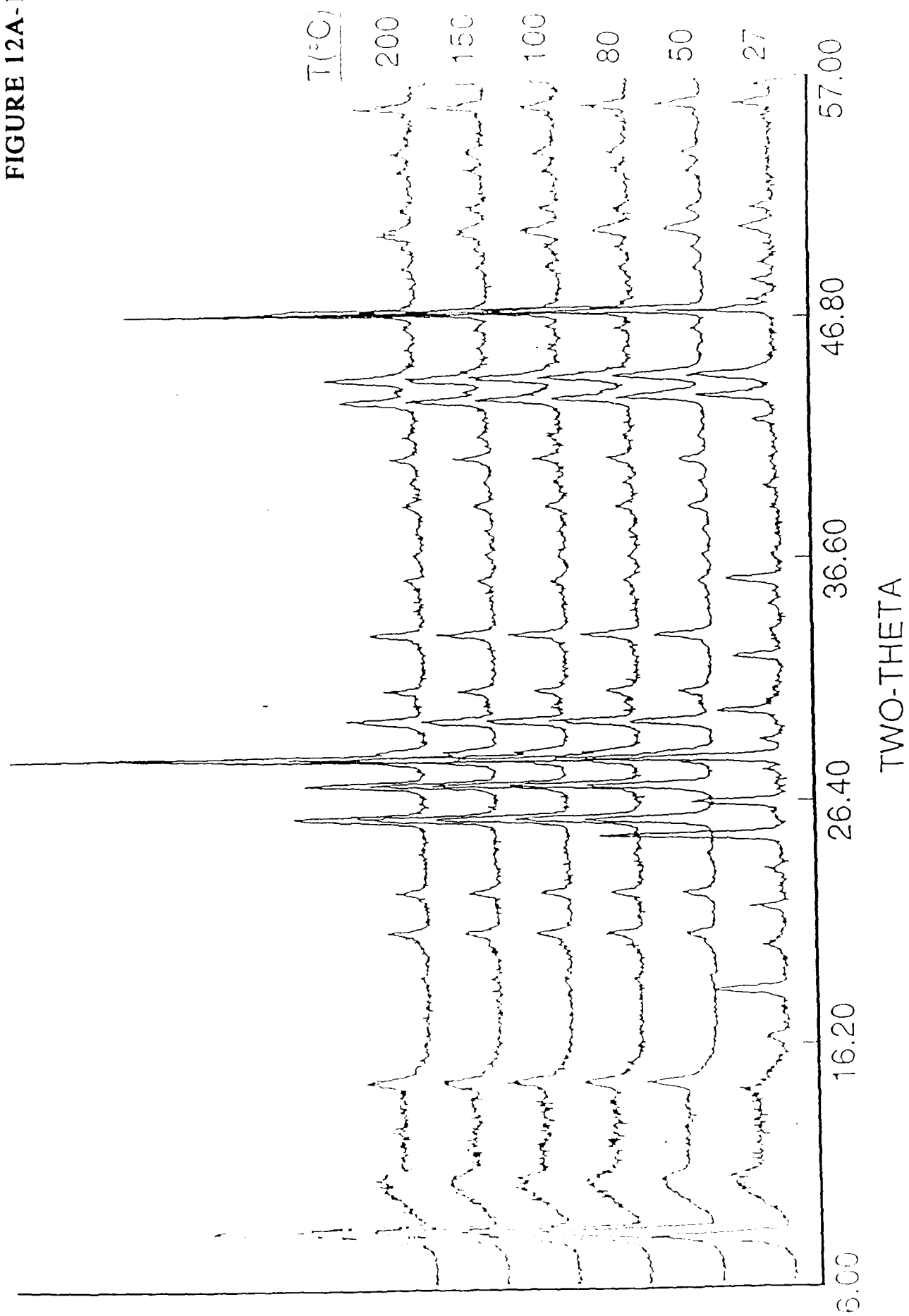


FIGURE 12A-2

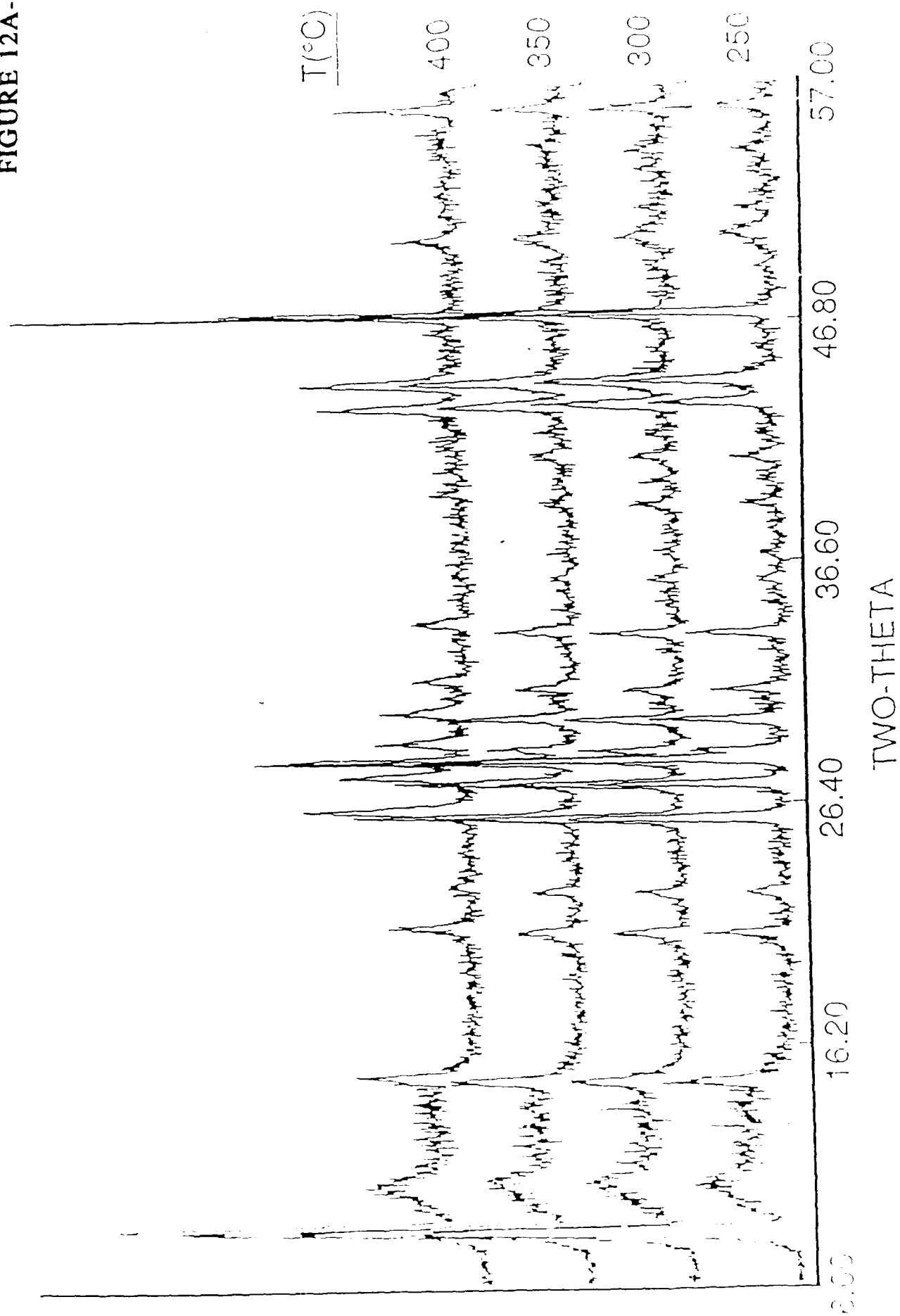


FIGURE 12B

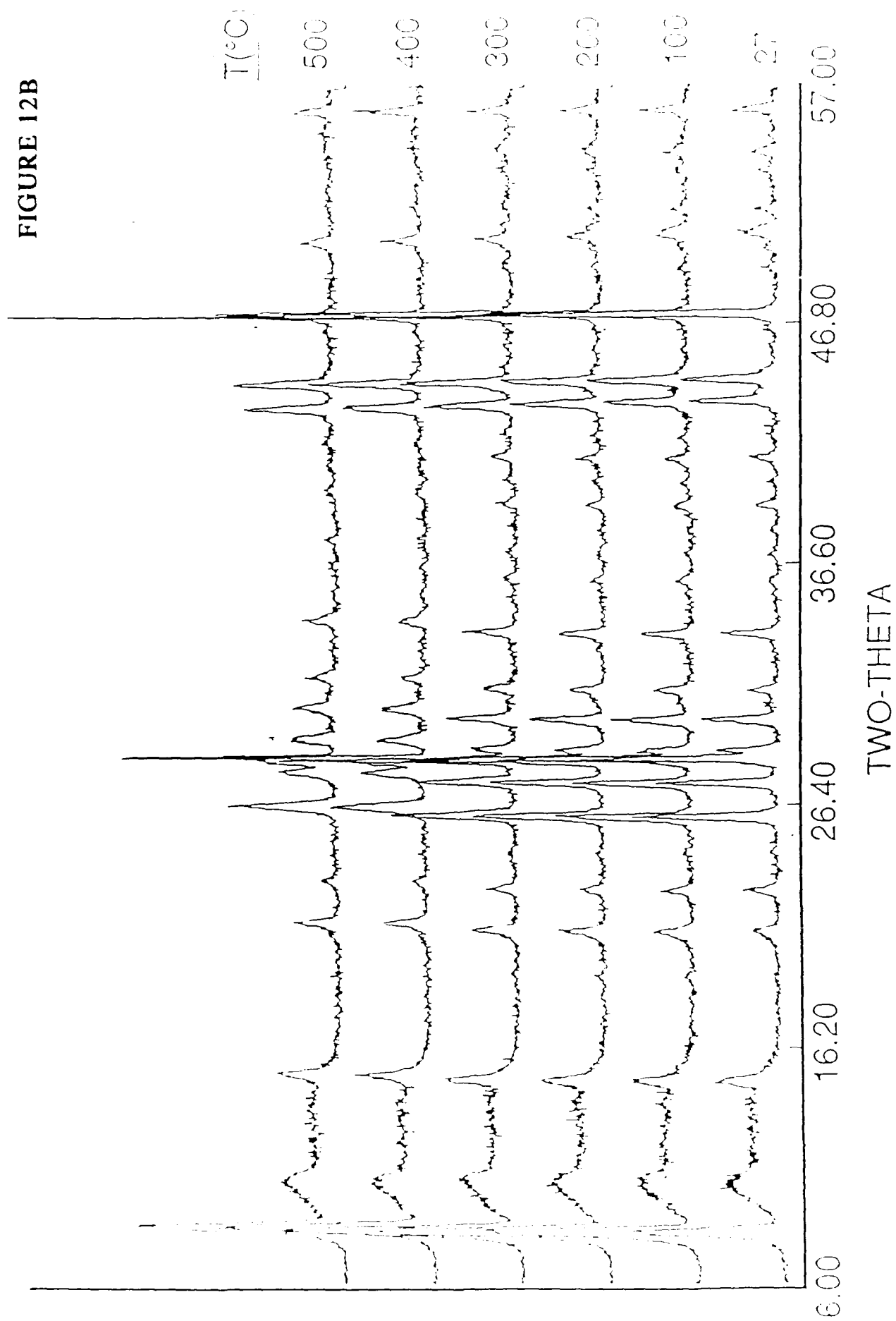


FIGURE 13A

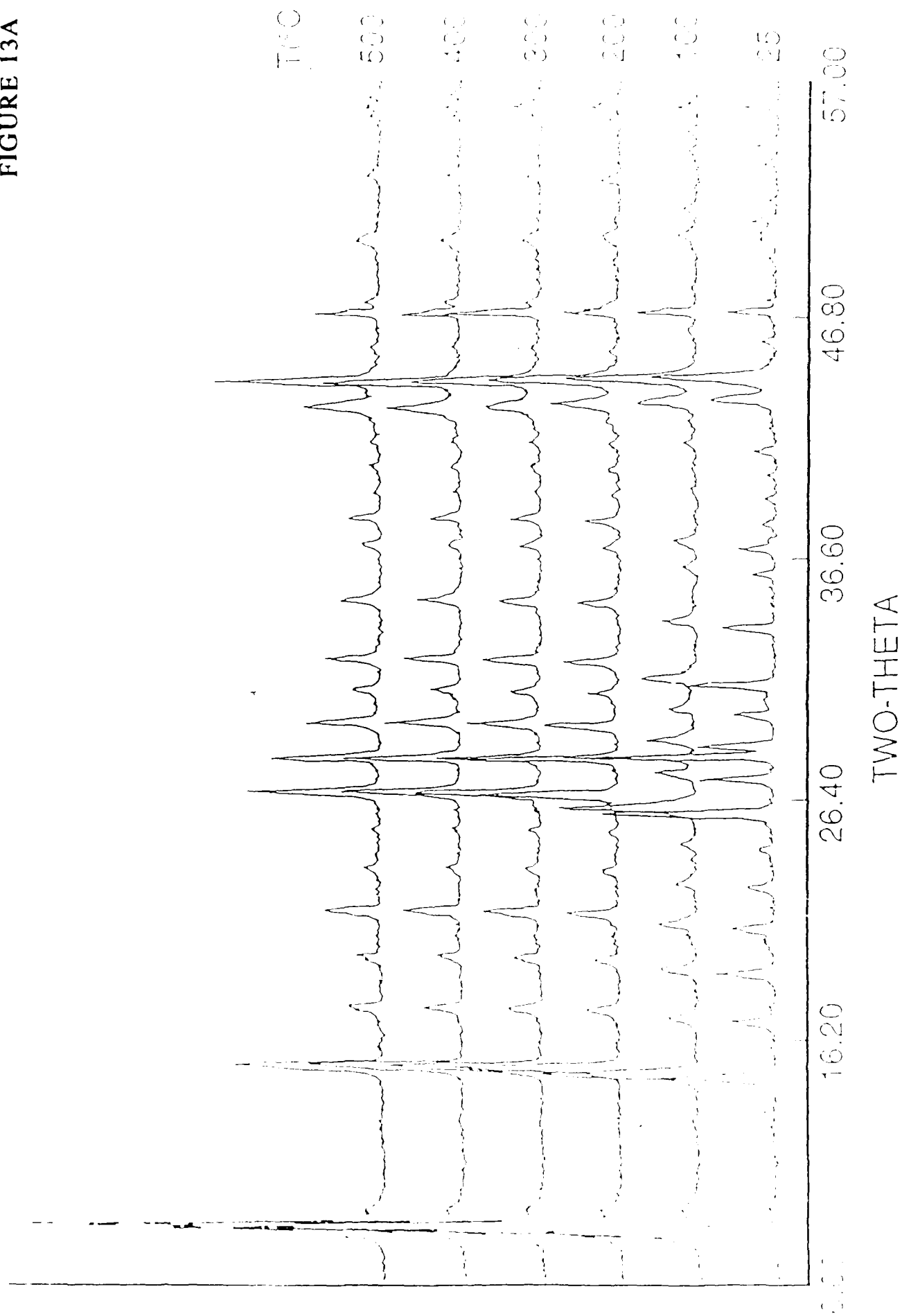


FIGURE 13B

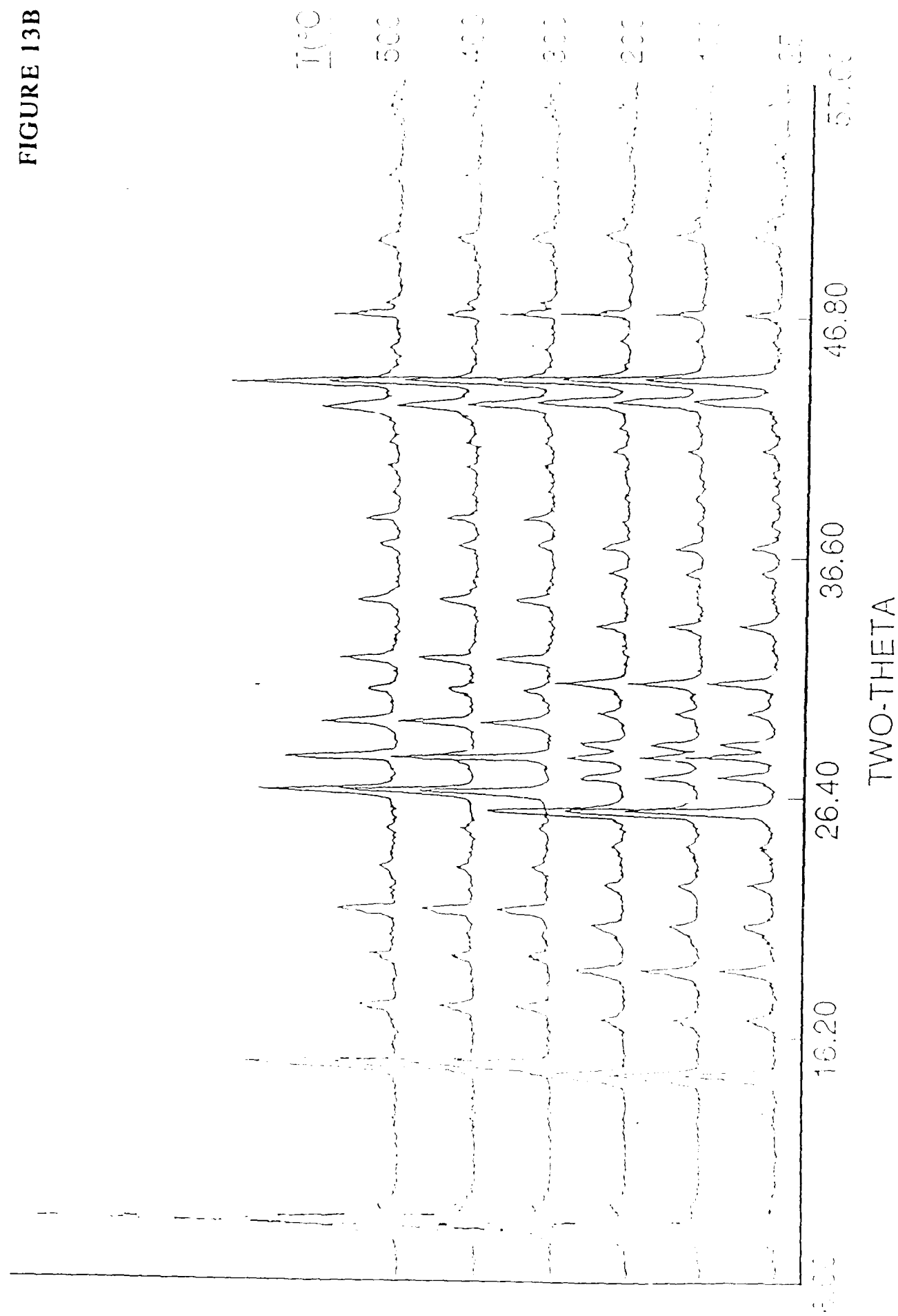


FIGURE 14A

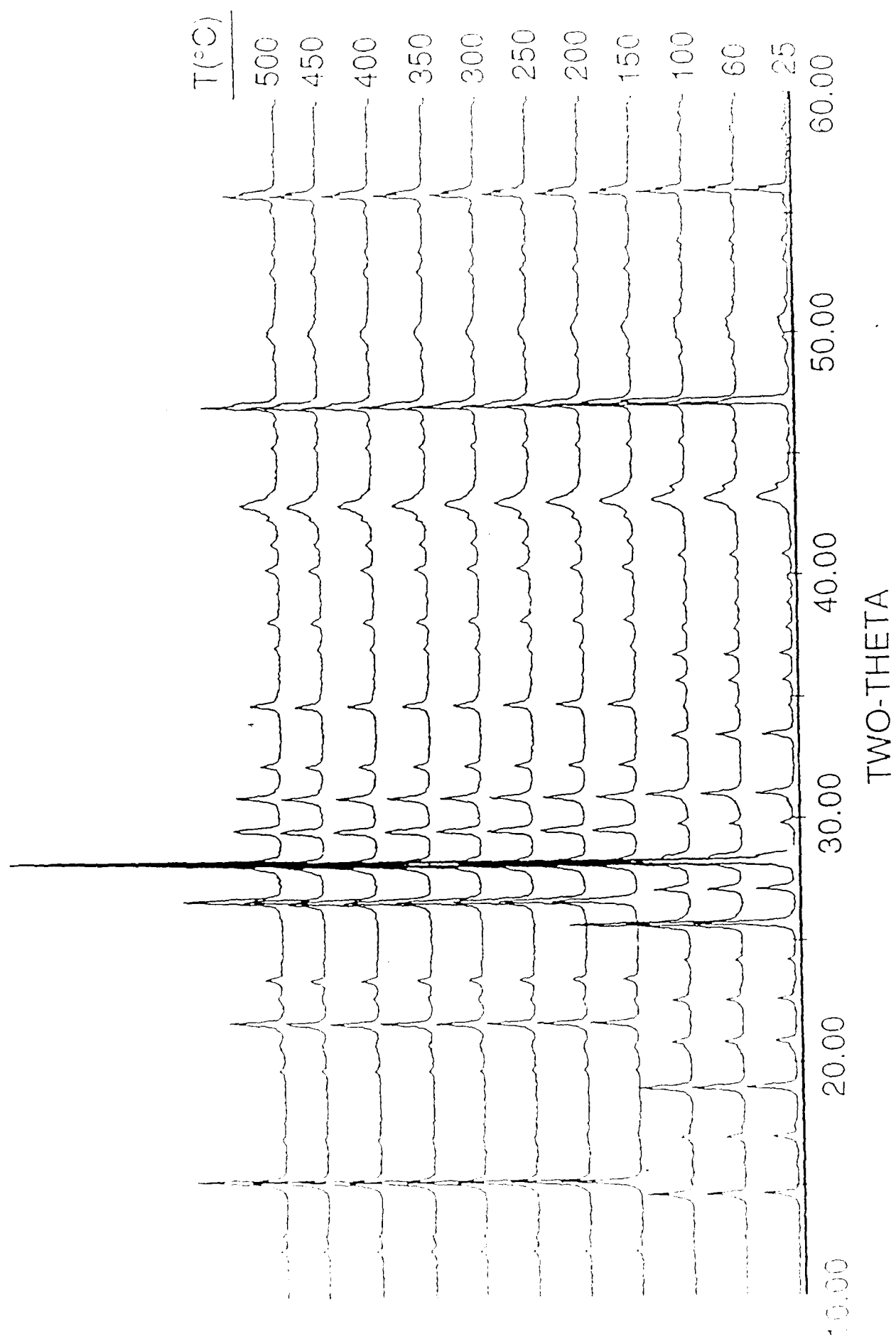


FIGURE 14B

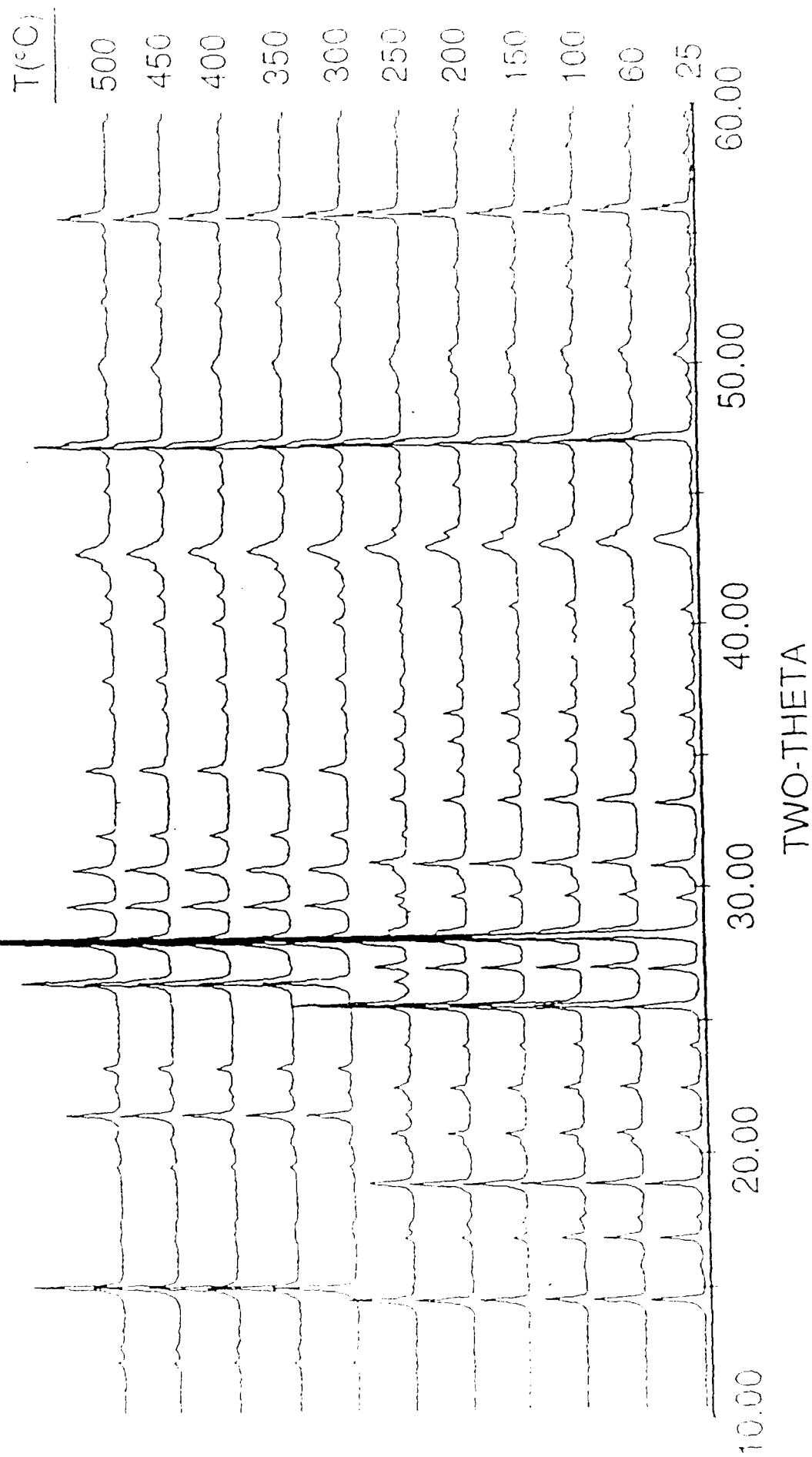


FIGURE 15A

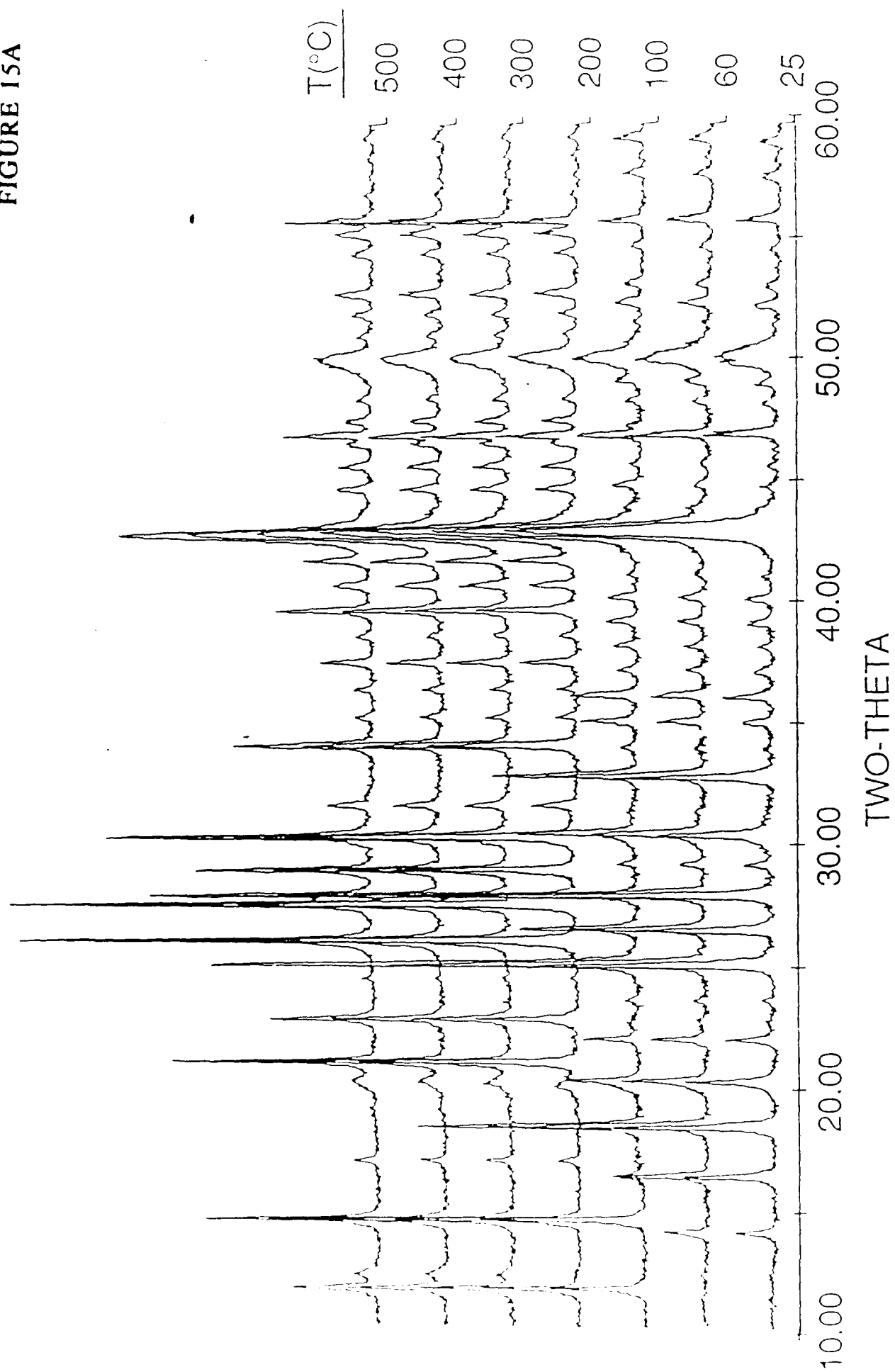


FIGURE 15B

